공학박사 학위논문

A study on phase transitional gel based on amine polymer for adhesives and microfluidic system

아민 계열 고분자 젤의 상 전이 통한 접착제 및 미세 유체 제어 연구

2023 년 2 월

서울대학교 대학원
재료공학부

이 호 준

A study on phase transitional gel based on amine polymer for adhesives and microfluidic system

아민 계열 고분자 젤의 상 전이 통한 접착제 및 미세 유체 제어 연구

지도 교수 선 정 윤

이 논문을 공학박사 학위논문으로 제출함

2022 년 12 월

서울대학교 대학원
재료공학부

이 호 준

이호준의 공학박사 학위논문을 인준함
2022 년 12 월

위 원 장	안 철 희	(인)
부위원장	선 정 윤	(인)
위 원	도 준 상	(인)
위 원	김 소 연	(인)
위 원	이 근 형	(인)

Abstract

With rapidly growing attention to hydrogels based on their unique characteristics, significant efforts to utilize them have been reported. Dual crosslinking model became a typical strategy to overcome weak and brittle properties of hydrogels. Besides, hydrogels started to be wrapped by hydrophobic materials in order to delay the dehydration. Then, various applications were explored using biocompatibility, stretchability, and stimuli responsivity, etc. However, there are still hurdles to become commercial materials with regard to methods and processes.

Here, we demonstrate that hydrogels can be more practical and facilely-used based on phase transition study. Precisely controlled phases and their characterizations supported that hydrogels are highly capable of becoming commercially utilized. Especially, we investigated adhesives and heavy metal removal system in depth.

In first part, strong and facile adhesives were demonstrated derived from systemically phase-controlled polyelectrolyte complexes (PAA/BPEI). Fluidic coacervates, an aggregate of oppositely charged polymers like colloids, were utilized when coating layer was loaded. Then, pH-induced phase transition from coacervate to gel contributed to enhancing adhesion strength. These facile methods attributed a uniform adhesive formation, so that it helped to analyze adhesion mechanism comprehensively. Then, thermal treatment was considered in order for the formation of chemically crosslinked gel. As a result, amide bond converted from carboxylic acid of PAA resulted in 2.4 MPa, which was the level of commercial products.

In second part, reversible crosslinking of chitosan/Cu^{2+} was studied regarding recyclable heavy metal removal system. Different from the previous works, we intended to enhance the dissolution rate of coordinate complexes, because this approach was strongly related with the process of hydrogel regeneration. Based on the metal-ion

affinity of organic molecules, it was found that nitrite considerably accelerated the extraction of Cu^{2+} from chitosan. Lastly, microfluidic switch was newly demonstrated using reversible crosslinking of polymer/metal−ion complexes.

Keyword: hydrogels, phase transition, polyelectrolyte, coordinate complexes, adhesives, microfluidics

Student Number: 2019−33177

Table of Contents

List of Tables

List of Figures

Chapter 1. Introduction

1.1. Study background

1.1.1. Hydrogel

A hydrogel, composed of water and hydrophilic polymer, is a three-dimensional network of elastic solid.[1-3] This unique polymer structure was first reported by Wichterle and Lím in 1960.[4] By definition, hydrogels must contain water with an aid of the hydrophilic groups such as amine, carboxyl, hydroxyl, and amide, etc.

Crosslinked polymer chains within water molecules render hydrogels into unique characteristics. Stretchability and softness are typical examples of hydrogels. The configuration of the polymer network can be adjusted, so that it can endure mechanical strain of up to 1000 %.[5] Also, the elastic modulus of hydrogels is in the range from 1 to 100 kPa, which is softer than that of other compliant materials. This is explained by the large volume fraction of water.[2,6] In fact, hydrogels can hold a large amount of water while maintaining the structure due to chemical or physical crosslinking of individual polymer chains. Furthermore, non-toxic hydrophilic polymers can become biocompatible hydrogels.[3,7] Thus, they can be introduced into the field of biological as well as cosmetic applications.[8-10] Interestingly, hydrogels can respond to diverse external stimuli via interactions between the polymer network and water, so that they are expected to be a promising material with increased functionality.[11-13]

1.1.2. Issues and challenges

Although hydrogels are mostly stretchable and soft, they are also easily broken caused by high water content.[14-15] This issue has restricted their applications, so that how to enhance mechanical properties of hydrogels has been a great challenge. Normal hydrogels exhibit a sub-MPa tensile stress and approximately one hundredth fracture energy of biological tissues such as cartilage.[16] Therefore,

some researchers started to design network structures of hydrogels, such as double network hydrogels and nanocomposite hydrogels.[5,17–20] As reported, double network energy dissipation model considerably attributes to enhanced mechanical properties resulting in tough gel.[17]

Based on unique characteristics of hydrogels, there have been significant efforts to excavate application fields. They offer a broad range of potential applications such as biomedical,[8–10] environmental,[21–23] robotics,[6,24–26] electronics,[27–29] and functional coating,[30–32] etc. In brief, antimicrobial and biocompatible properties attribute to medical approach including wound management and tissue engineering. Further, hydrogels, which are capable of forming coordinate complexes, can be utilized as water purification system or membrane. In addition, actuator and electronics have been reported based on stimuli responsivity and transparency, respectively. Functional coating is also regarded as a practical field, such as polyelectrolyte complexes layer for adhesives or gas barrier.

By all means, there have been still significant challenges. For example, hydrogels should be treated to delay the dehydration when they are exposed to a dry environment.[33,34] Furthermore, fabrication process as well as mass production are significant issues, because these will be hurdles to commercialize hydrogels in the near future. Fortunately, a few researchers started to discuss the methods dealing with scalable and cost–effective fabrications of hydrogels. Also, key process factors were analyzed in–depth in order to control the performances of hydrogels.[35–40] However, more specific approaches seemed to be helpful considering well–established polymer engineering fields such as solvent casting and coating. On the other hand, recyclable and reusable hydrogel systems need to be developed in earnest. Even though these merits are one of the fascinating properties, previous works tended to only focus on the gelation and the performance of hydrogels. In order to become eco–friendly materials, it is considerably important to design the process of hydrogel regeneration.[41–44]

1.2. Purpose of research

1.2.1. Goals

This dissertation tried to study phase behaviors of physically crosslinked hydrogels in quantitative to utilize hydrogels more practical. To be more specific, precise phase control for advanced coating process and reversible crosslinking for recycle material are interests. In terms of material, amine-based hydrophilic polymers are selected, because this functional group shows various physical bond. For dynamic and reversible phase transition study, amine is most suitable. This dissertation is composed of two parts.

1.2.2. Outline

In Chapter 2, the factors of polyelectrolyte adhesives were precisely investigated in terms of electrostatic interaction using conventional rod coating and pH-induced phase transition, followed by a phase study between poly(acrylic acid) and branched poly(ethylenimine). The phase was systemically controlled by parameters such as polymer ratio, concentration of NaCl, and pH level. Then, the rheological modulus of each phase was studied to understand physical cross-linking. In relation to polyelectrolyte adhesives, it was found that a higher viscous phase led to more intensive adhesion strength. In addition, thermal treatment helped to obtain a dramatic increase in adhesion strength (2.4 MPa), which was accomplished by a conversion reaction from carboxylic acid to amide. This chemically cross-linked gel adhesive performance could compete with commercial grade adhesive, and this study creates a pathway to design polyelectrolyte adhesive regarding a facile process and applications.

In Chapter 3, dynamic studies of the dissolution as well as the gelation of a physically crosslinked chitosan hydrogel were presented. Specifically, a one-dimensional gel growth system and an acetate buffer solution were prepared for the precise analysis of the dominant factors affecting a phase transition. The dissolution rate

was found to be regulated by three major factors of the pH level, Cu^{2+}, and NO_2^-, while the gelation rate was strongly governed by the concentration of OH^-. Apart from the gelation rate, the use of Cu^{2+} led to the rapid realization of gel characteristics. The results here provide strategies for process engineering, ultimately to determine the phase-transition rates. In addition, a microfluidic switch was successfully operated based on a better understanding of the reversible crosslinking of the chitosan hydrogel. Rapid gelation was required to close the channel, and a quick switchover was achieved by a dissolution enhancement strategy. As a result, factors that regulated the rates of gelation or dissolution were found to be useful to operate the fluidic switch.

Reference

(1) Lee, H.-R.; Kim, C.-C.; Sun, J.-Y. Stretchable Ionics - A Promising Candidate for Upcoming Wearable Devices. Adv. Mater. 2018, New J. Chem. 2018, 30, 1704403.

(2) Yang, C.; Suo, Z. Hydrogel Ionotronics. Nat. Rev. Mater. 2018, 3, 125-142.

(3) Yuk, H.; Lu, B.; Zhao, X. Hydrogel Bioelectronics. Chem. Soc. Rev. 2019, 48, 1642-1667.

(4) Wichterle, O.; Lim, D. Hydrophilic Gel for Biological Use. Nature 1960, 185, 117-118.

(5) Sun, J.-Y.; Zhao, X.; Illeperuma, W. R. K.; Chaudhuri, O.; Oh, K. H.; Mooney, D. J.; Vlassak, J. J.; Suo, Z. Highly Stretchable and Tough Hydrogels. Nature 2012, 489, 133-136.

(6) Lee, Y.; Song, W. J.; Sun, J.-Y. Hydrogel Soft Robotics. Mater. Today Phys. 2020, 15, 100258.

(7) Applegate, M. B.; Coburn, J.; Partlow, B. P.; Omenetto, F. G. Laser-Based Three-Dimensional Multiscale Micropatterning of Biocompatible Hydrogels for Customized Tissue Engineering Scaffolds. Proc. Natl. Acad. Sci. U.S.A. 2015, 112, 12052-12057.

(8) Daly, A. C.; Riley, L.; Segura, T.; Burdick, J. A. Hydrogel Microparticles for Biomedical Applications. Nat. Rev. Mater. 2020, 5, 20-43.

(9) Liao, Y.; Xie, L.; Ye, J.; Chen, T.; Huang, T.; Shi, L.; Yuan, M. Sprayable Hydrogel for Biomedical Applications. Biomater. Sci. 2022, 10, 2759-2771.

(10) Zhang, Y.; Wang, Y.; Wen, Y.; Zhong, Q.; Zhao, Y. Self-Healable Magnetic Structural Color Hydrogels. ACS Appl. Mater. Interfaces 2020, 12, 7486-7493.

(11) Willner, I. Stimuli-Controlled Hydrogels and Their Applications. ACS. Chem. Res. 2017, 50, 657-658.

(12) Zhang, D.; Ren, B.; Zhang, Y.; Xu, L.; Huang, Q.; He, Y.; Li, X.; Wu, J.; Yang, J.; Chen, Q.; Chang, Y.; Zheng, J. From Design to Applications of Stimuli-Responsive Hydrogel Strain Sensors. J. Mater. Chem. B 2020, 8, 3171-3191.

(13) Hu, X.; Mclntosh, E.; Simon, M. G.; Staii, C.; Thomas III, S. W. Stimuli-Responsive Free-Standing Layer-By-Layer Films. Adv. Mater. 2016, 28, 715-721.

(14) Lake, G. J.; Thomas, A. G. The Strength of Highly Elastic Materials. Proc. R. Soc. 1967, 300, 108-119.

(15) Lin, X.; Zhao, X.; Xu, C.; Wang, L.; Xia, Y. Progress in the Mechanical Enhancement of Hydrogels: Fabrication Strategies and Underlying Mechanisms. J. Polym. Sci. 2022, 60, 2525-2542.

(16) Simha, N. K.; Carlson, C. S.; Lewis, J. L. Evaluation of Fracture Toughness of Cartilage by Micropenetration. J. Mater. Sci. Mater. Med. 2003, 14, 631-639.

(17) Gong, J. P.; Katsuyama, Y.; Kurokawa, T.; Osada, Y. Double-Network Hydrogels with Extremely High Mechanical Strength. Adv. Mater. 2003, 15, 1155-1158.

(18) Gong, J. P. Why are Double Network Hydrogels so Tough? Soft Matter 2010, 6, 2583-2590.

(19) Ma, J.; Lee, J.; Han, S. S.; Oh, K. H.; Nam, K. T.; Sun. J.-Y. Highly Stretchable and Notch-Insensitive Hydrogel Based on Polyacrylamide and Milk Protein. ACS. Appl. Mater. Interfaces 2016, 8, 29220-29226.

(20) Nan, J.; Zhang, G.; Zhu, T.; Wang, Z.; Wang, L.; Wang, H.; Chu, F.; Wang, C.; Tang, C. A Highly Elastic and Fatigue-Resistant Natural Protein-Reinforced Hydrogel Electrolyte for Reversible Compressible Quasi-Solid-State Supercapacitors. Adv. Sci. 2020, 7, 2000587.

(21) Basak, S.; Nandi, N.; Paul, S.; Hamley, I. W.; Banerjee, A. A Tripeptide-Based Self-Shrinking Hydrogel for Waste-Water Treatement: Removal of Toxic Organic Dyes and Lead (Pb^{2+}) Ions. Chem. Commun. 2017, 53, 5910-5913.

(22) Nie, J.; Wang, Z.; Hu, Q. Chitosan Hydrogel Structure Modulated by Metal Ions. Sci. Rep. 2016, 6, 36005.

(23) Jayakumar, A.; Jose, V. K.; Lee, J.-M. Hydrogels for Medical and Environmental Applications. Small Methods2020, 4, 1900735.

(24) Na, H.; Kang, Y.-W.; Park, C. S.; Jung, S.; Kim, H.-Y.; Sun, J.-Y. Hydrogel-Based Strong and Fast Actuators by Electroosmosis Turgor Pressure. Science 2022, 376, 301-307.

(25) Rus, D.; Tolley, M. T. Design, Fabrication and Control of Soft Robots. Nature 2015, 521, 467-475.

(26) Lee, Y.; Song, W. J.; Jung, Y.; Yoo, H.; Kim, M.-Y.; Kim, H.-Y.; Sun, J.-Y. Ionic Spiderwebs. Sci. Robot. 2020, 5, aaz5405.

(27) Keplinger, C.; Sun, J.-Y.; Foo, C. C.; Rothemund, P.; Whitesides, G. M.; Suo, Z. Stretchable, Transparent, Ionic Conductors. Science

2013, 341, 984–987.

(28) Kim, C.–C.; Lee, H.–H.; Oh, K. H.; Sun, J.–Y. Highly Stretchable, Transparent Ionic Touch Panel. Science 2016, 353, 682–687.

(29) Lee, Y.; Cha, S. H.; Kim, Y.–W.; Choi, D.; Sun, J.–Y. Transparent and Attachable Ionic Communicators Based on Self–Cleanable Triboelectric Nanogenerators. Nat. Commun. 2018, 9, 1804.

(30) Gan, D.; Xing, W.; Jiang, L.; Fang, J.; Zhao, C.; Ren, F.; Fang, L.; Wang, K.; Lu, X. Plant–Inspired Adhesives and Tough Hydrogel Based on Ag–Lignin Nanoparticles–Triggered Dynamic Redox Catechol Chemistry. Nat. Commun. 2019, 10, 1487.

(31) Wei, L.; Huang, J.; Yan, Y.; Cui, J.; Zhao, Y.; Bai, F.; Liu, J.; Wu, X.; Zhang, X.; Du, M. Substrate–Independent, Mechanically Tunable, and Scalable Gelatin Methacryloyl Hydrogel Coating with Drag–Reducing and Anti–Freezing Properties. ACS Appl. Polym. Mater. 2022, 4, 4876–4885.

(32) Yao, X.; Liu, J.; Yang, C.; Yang, X,; Wei, J.; Xia, Y.; Gong, X.; Suo, Z. Hydrogel Paint. Adv. Mater. 2019, 31, 1903062.

(33) Mredha, M. T. I.; Le, H. H.; Cui, J.; Jeon, I. Double–Hydrophobic–Coating through Quenching for Hydrogels with Strong Resistance to Both Drying and Swelling. Adv. Sci. 2020, 7, 1903145.

(34) Floch, P. L.; Yao, X.; Liu, Q.; Wang, Z.; Nian, G.; Sun, Y.; Jia, L.; Suo, Z. Wearable and Washable Conductors for Active Textiles. ACS Appl. Mater. Interfaces 2017, 9, 25542–25552.

(35) Yu, A. C.; Chen, H.; Chan, D.; Appel, E. A. Scalable Manufacturing of Biomimetic Moldable Hydrogels for Industrial

Applications. Proc. Natl. Acad. Sci. U.S.A. 2016, 113, 14255−14260.

(36) Chen, G.; Li, T.; Chen, C.; Kong, W.; Jiao, M.; Jiang, B.; Xia, Q.; Liang, Z.; Liu, Y.; He, S.; Hu, L. Scalable Wood Hydrogel Membrane with Nanoscale Channels. ACS Nano 2021, 15, 11244−11252.

(37) Zhu, M.; Wang, Y.; Ferracci, G.; Zheng, J.; Cho, N.−J.; Lee, B. H. Gelatin Methacryloyl and its Hydrogels with an Exceptional Degree of Controllability and Batch−to−Batch Consistency. Sci. Rep. 2019, 9, 6863.

(38) Li, H.; Teng, C.; Zhao, J.; Wang, J. A Scalable Hydrogel Processing Route to High Strength, Foldable Clay−Based Artificial Nacre. Compos. Sci. Technol. 2021, 201, 108543.

(39) Yoo, P. J.; Zacharia, N. S.; Doh, J.; Nam, K. T.; Belcher, A. M.; Hammond, P. T. Controlling Surface Mobility in Interdiffusing Polyelectrolyte Multilayers. ACS Nano 2008, 2, 561−571.

(40) Kim, H. J.; Yang, H. M.; Koo, J.; Kang, M. S.; Hong, K.; Lee, K. H. Area−Controllable Stamping of Semicrystalline Copolymer Ionogels for Solid−State Electrolyte−Gated Transistors and Light−Emitting Devices. ACS Appl. Mater. Interfaces 2017, 9, 42978−42985.

(41) Cai, Y.; Zheng, L.; Fang, Z. Selective Adsorption of Cu(II) from an Aqueous Solution by Ion Imprinted Magnetic Chitosan Microspheres Prepared from Steel Pickling Waste Liquor. RSC Adv. 2015, 5, 97435−97445.

(42) Perumal, S.; Atchudan, R.; Yoon, D. H.; Joo, J.; Cheong, I. W. Spherical Chitosan/Gelatin Hydrogel Particles for Removal of Multiple Heavy Metal Ions from Wastewater. Ind. Eng. Chem. Res. 2019, 58, 9900−9907.

(43) Saad, A. H. A.; Azzam, A. M.; El-Wakeel, S. T.; Mostaf, B. B.; El-latif, M. B. A. Removal of Toxic Metal Ions from Wastewater Using ZnO@Chitosan Core-Shell Nanocomposite. Environ. Nanotechnol. Monit. Mang. 2018, 9, 67-75.

(44) Zhang, K.; Luo, X.; Yang, L.; Chang, Z.; Luo, S. Progress toward Hydrogels in Removing Heavy Metals from Water: Problems and Solutions. ACS EST Water 2021, 1, 1098-1116.

Chapter 2. Strong and facile adhesives based on phase transitional polyelectrolytes

2.1. Introduction

The polyelectrolyte complex is a 3-dimensional electrostatic network that is composed of oppositely charged polymers.[1-3] On the basis of its unique characteristics such as hydrophilicity, biocompatibility, and stimuli-responsivity, a wide range of applications including membranes, biosensors, and smart actuators have been developed.[4-11] Furthermore, the stickiness of this material driven by electrostatically charged surfaces has gradually inspired potential applications of polyelectrolyte complexes as adhesives.[12-17]

Polyelectrolyte complexes have three different phases, namely, gel (solid), coacervate (colloidal suspension), and sol (completely dissolved solution).[18-22] **Figure 2.1a** describes these typical phases determined by a controlled electrostatic interaction. Here, the addition of salt tends to hinder electrostatic cross-linking between oppositely charged polymers. Therefore, polymer chains become more hydrated as the amount of salt increases, which will influence the rheological behaviors and adhesion. In the case of sol, polymer chains could not participate in physical binding, so they become dissolved in aqueous solution. On the other hand, polymer chains of two phases, except sol, result in an electrostatic network and become capable of joining two substrates by electrostatic binding. Therefore, previous works focused on the adhesive performance of gel or coacervate, respectively.[12-17] For example, Zhang et al. reported the adhesion energy of 2180 J/m^2 (hydrogel substrate) using polyelectrolyte gel composed of poly(acrylic acid) and poly(ethylenimine).[16] Also, Gao et al. suggested adhesive coacervate driven by natural biomolecule, which showed an adhesion strength of 33 and 139 kPa for polymer and glass substrate, respectively.[17] However, they scarcely discussed the effect of polyelectrolyte

phases as well as rheological analysis, which are essential to uncover the origin of the adhesion properties. This reveals that more fundamental and detailed approaches to polymer adhesive are still required for a comprehensive understanding.

Previous studies offer excellent hints to investigate adhesion properties in-depth.[22-27] For example, Li et al. tried to apply coacervates composed of poly(acrylic acid) and branched poly(ethylenimine) for the coating solution on poly(propylene) film.[22] In a similar manner, Haile et al. and Smith et al. suggested the way to obtain a more intensive layer is by immersing coacervate in the desired pH level.[23,24] As a result, they successfully fabricated an oxygen barrier layer using the conventional coating method and pH level control. These reports present that the polyelectrolyte adhesion properties could be systemically studied with the help of a facile process and precise phase control.

If further steps could provide outstanding performance without material change, the polyelectrolyte adhesive system would be considered as more applicable and practical. In the case of poly(acrylic acid) and poly(ethylenimine), they are able to chemically cross-link by the formation of amide bonding,[28-30] so that adhesion strength could be enhanced. This conversion from carboxylic acid to amide is known to occur at elevated temperatures without the addition of catalyst.[28,29] We believe that this simple approach will be regarded as a new trial for polymer adhesive design and be applicable for various purposes.

Here, we have conducted a phase study of polymer complexes composed of poly(acrylic acid) and branched poly(ethylenimine) with different parameters such as polymer ratio, concentration of NaCl, and pH level. Precisely controlled conditions and rheological analysis contribute to a better understanding of phase behavior in terms of electrostatic interaction. In particular, each phase was quantitatively identified using complex viscosity, which was the novel approach to define the phase of polyelectrolyte. Then, the conventional coating method and pH-induced phase transition were introduced to

physically join two substrates. In addition, thermal treatment was considered for the formation of chemical cross-linking. On the basis of phase transitional polyelectrolyte complexes, the adhesion strengths were analyzed in detail.

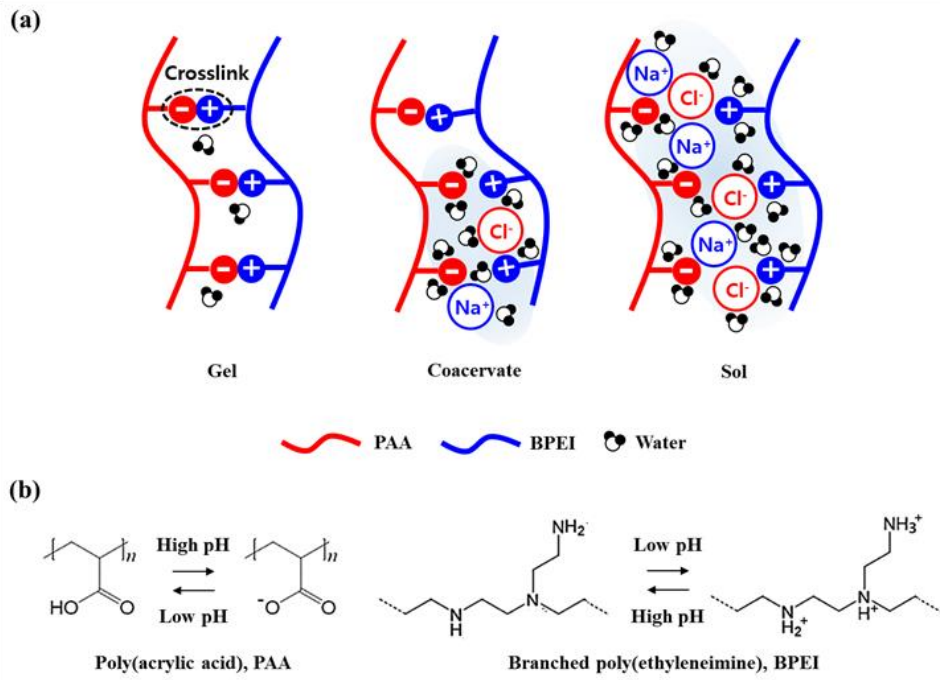

Figure 2.1. Phase transition of PAA and BPEI solution: (a) Schematic of the microstructures of polyelectrolytes such as gel, coacervate, and sol. Here, NaCl impacts the solubility of polymers, because an increase in ionic strength causes a decrease in electrostatic interaction between charged polymers. Therefore, polymer chains become more hydrated as increased amount of NaCl, which influences on rheological behavior and adhesion. (b) Poly(acrylic acid) as an anionic polymer (pKa 4.5) and branched poly(ethyleneimine) as a cationic polymer (pKa = 4.5, 6.7, and 11.6).

2.2. Experimental section

2.2.1. Materials

Poly(acrylic acid) (PAA; average Mw of 1800 g/mol), branched poly(ethylenimine) (BPEI; average Mw of 25000 g/mol), sodium chloride (NaCl), hydrochloric acid (HCl; ACS reagent, 37%), anhydrous sodium hydroxide (NaOH; ACS reagent, ≥97.0%), citric acid monohydrate ($C_6H_8O_7 \cdot H_2O$), and sodium citrate dihydrate ($C_6H_5Na_3O_7 \cdot {}_{2H2O}$) were purchased from Sigma-Aldrich. All chemicals were used as received.

2.2.2. PAA/BPEI complexes phase study

2.2.2.1. Preparation of polymer solutions before mixing. All aqueous solutions were prepared with deionized water. Next, NaCl was added into individual 10 wt % aqueous solutions of PAA and BPEI for the desired concentration of NaCl. Then, 5 M aqueous solutions of HCl and NaOH were used to adjust the pH levels. For each polymer solution (PAA or BPEI), 50 sets with different concentrations of NaOH (0.0-2.8 M) and pH levels (1-10) were prepared.

2.2.2.2. Mixing polymer solutions. The BPEI solution was added dropwise into the PAA solution with the same concentration of NaCl and pH level, while stirring vigorously at a speed of 300 rpm at room temperature (RT). The ratios between PAA and BPEI (PAA/BPEI) were controlled from 10 to 90 wt %. Then, the final concentrations of polymer mixtures (PAA+BPEI) were precisely calculated considering the change in mass during pH level adjustment of 4.9 ± 0.2 wt %.

2.2.2.3. Phase identification. After the mixtures were stirred for an additional 10 min, three different phases could be obtained. In detail, they were identified as a gel when a white solid was observed; meanwhile, sol completely dissolved in solution. For coacervate formation, the turbid solution (prestate of coacervate) was additionally annealed for 4 h at 80 °C. During the annealing, the polymer-dense region became separated from the polymer-dilute region. Then, coacervate was finally prepared, and it could be

regarded as a viscous liquid. To define the phase quantitatively, the relative turbidity and the complex viscosity were analyzed. We measured the relative turbidity before annealing using a Turbiscan Lab (Formulaction, France). Then, the relative turbidity was calculated from incident light intensity (I_0) and the intensity of light passed through samples (I): $\boldsymbol{relative\ turbidity} = -ln\frac{I}{I_o}$. Also, the complex viscosity (η^*) of lower than 0.25 Pa · s, while gel tended to show a higher viscosity than coacervate.

2.2.3. Lap Shear adhesion test

2.2.3.1. Preparation of coacervate adhesive sample. For an adhesive layer deposition, coacervates with different polymer ratios (PAA/BPEI), concentrations of NaCl, and pH levels were prepared. Then, coacervate was deposited on a pair of corona-treated PET films using a #18 Mayer rod (R.D. Specialties, US). Another part was placed on top of the first part to form a lap shear joint of 20 mm × 10 mm, and the adhesive area was pressed with a 20 g weight (1000 N/m^2) for 2 h at RT. The final dimensions of the samples were fixed at 70 mm × 20 mm (length × width).

2.2.3.2. Preparation of gel adhesive sample. All processes were the same as described in Section 2.2.3.1 before the formation of a lap shear joint. After the deposition, 1 M citrate aqueous buffer solutions with pH levels of 3, 4, and 5 were prepared. Then, following coacervate deposition, a pair of PET films were dipped in buffer solution for 30 s for pH-induced phase transition from coacervate (transparent) to gel (opaque).

2.2.3.3. Preparation of thermally treated adhesive sample. The fabricated samples described in Sections 2.2.3.1 and 2.2.3.2 were heated at 135 ℃ for 4 h with a pressure of 1000 N/m^2. Then, all samples were stored in the chamber with a relative humidity of 90% RH at 40 ℃ for 1 day.

2.2.3.4. Measurement of lap shear adhesion strength. Adhesion strengths of the PAA/BPEI complex adhesives were determined

using Instron 2580 Instrument (Instron, US) equipped with a 5 kN load cell. The lap shear test was performed with a crosshead speed of 10 mm/min until full separation. For each type of adhesive, at least 5 samples were tested, and the result was summarized with the average values. Substrates made of glass and rubber were tested as well, all of which were fabricated by the same process. For repeatable adhesion tests of physically cross-linked adhesives such as coacervate and gel, the pressure of 1000 N/m^2 lasted for 30 min, followed by a drop of citrate buffer solution (100 mL/m^2) being applied on the detached adhesive surface to adhere substrates during each attachment. Each detachment was carried out by the lap shear test.

2.2.4. Characterization

2.2.4.1. Rheology. To define the three different phases quantitatively, rheological analysis was performed with an Advanced Rheometric Expansion System (Rheometric Scientific, UK) in a parallel plate configuration. Dynamic frequency sweep (25 °C, 0.5 % strain) presented the values of storage modulus (G') and loss modulus (G'') at frequencies (ω) from 1 to 400 s^{-1}. Then, the complex viscosity (η^*) at each frequency was calculated from the measured G' and G'' as follows: $\textit{complex viscosity}\left(\eta^*\right) = \sqrt{(\frac{G'}{\omega})^2 + (\frac{G''}{\omega})^2}$.

2.2.4.2. FTIR-ATR. To identify chemical changes after thermal treatment, Fourier transform infrared spectra with attenuated total reflectance (FTIR-ATR) were recorded on a Nicolet iS10 (Thermo Scientific, US). The samples were prepared by the process described in Section 2.2.3.3, except that PAA/BPEI complexes were only loaded onto glass without any cover.

2.2.4.3. Swelling ratio. To measure the swelling ratio of the thermally treated adhesive layer, samples were prepared by the process described in Section 2.2.4.2. All samples were stored in the chamber with a relative humidity of 90 % RH at 40 °C for 1 day. Then, the swelling ratio was calculated by comparing the weights of

dried states (W_d) with swollen states at a n equilibrium (W_s) a s follows: $swelling\ ratio = \frac{W_s - W_d}{W_d}$.

2.2.4.4. Contact angle. Contact angles of PAA/BPEI complexes and substrates were measured with a Phoenix 300Touch (Surface Electro Optics, South Korea). Water droplets of 0.1 μL were generated by a glass syringe operation and allowed to impact the substrates. Then, the contact angle was recorded by a high-speed camera (84 frame/s) within 5 s.

2.2.4.5. Surface roughness. The values of Ra (center line average height) were calculated from the roughness profiles of the substrates using a Surfcorder ET4000A (Kosaka, Japan). Basically, the probe traveled across the substrate in the transverse direction.

2.3. Results and discussion

2.3.1. Phase study of PAA/BPEI complexes

As described in **Figure 1b**, poly(acrylic acid) (PAA) and branched poly(ethylenimine) (BPEI) were used as an anionic polymer (pKa 4.5) and a cationic polymer (pKa 4.5, 6.7, and 11.6), respectively. They were highly soluble in aqueous solution (more than 40 wt %) regardless of their charges, so that individual polymer solutions could be homogeneously prepared within the pH levels from 1 to 14. In particular, BPEI did not precipitate, while linear PEI was only soluble at low pH levels. Therefore, this polymer system was suitable for studying the phase behavior focusing on the electrostatic interaction between oppositely charged polymer chains.

To verify the phase behavior depending on parameters such as polymer ratio (PAA/BPEI), concentration of NaCl, and pH level, polymer mixtures were prepared first, as follows. Individual 10 wt % aqueous solutions of PAA and BPEI with the desired concentration of NaCl (0.0-2.8 M) and pH levels (1-10) were prepared, respectively. Then, each BPEI solution was added dropwise into the PAA solution with the same concentration of NaCl and pH level, while stirring vigorously at a speed of 300 rpm at RT. The amounts of solutions to

be mixed were determined by the polymer ratios ranging from 10 to 90 wt %. After stirring for an additional 10 min, mixtures with the final concentrations of 4.9 ± 0.2 wt % with respect to the polymers (PAA+BPEI) were obtained.

Three different phases were identified after polymer mixing and precipitation. Especially, both gel and coacervate required precipitation after polymer mixing. As shown in **Figure 2.2a, b**, the instant formation of a white color solid indicated a gel, while sol was completely dissolved in solution. A coacervate could be regarded as a colloidal suspension, and it showed viscous liquid-like characteristics. For coacervate formation, the viscous polymer-dense region should be separated from the polymer-dilute region through the annealing process. In fact, coacervate first appeared to be a turbid solution before a sedimentation due to an aggregate of oppositely charged polymers like colloids. Therefore, this phase was easily distinguished from a clear sol without the annealing process. As presented in **Figure 2.3b-d**, the relative turbidity of coacervate depended on the polymer ratio, while that of sol was nearly 0. Also, it could be found that a decrease in either concentration of NaCl or pH level led to an increase in the turbidity of coacervate. This was mainly because the relative turbidity was sensitive to the amount of coacervate in solution.[31] Therefore, the most turbid complex (60 wt % PAA, pH 6, 0.7 M NaCl) was expected to show the strongest adhesion strength as well as the highest complex viscosity among the coacervates. On the other hand, it was notable that a gel tended to settle down and shrank during the annealing process. However, it did not flow at room temperature due to its rigid and brittle properties. **Figure 2.3a** describes the overall annealing process and the appearance of three different phases. Especially, an example of annealed gel (60 wt % PAA, pH 5, 0.7 M NaCl) demonstrated that this phase still remained rigid and stagnant at room temperature. In case of a sol state, no phase separation was observed when sol was annealed.

One aspect that is exhibited in **Figure 2.2b** is the distinct shapes of gel the depending on the pH levels. For example, a large agglomeration was formed at pH 5, while separated beads were observed at pH 3. This implied that the electrostatic interaction between PAA and BPEI at pH 5 was stronger, compared to that at pH 3. Similarly, the gel tended to be more gummy and rigid than coacervate, as shown in **Figure 2,2c, d**, which could also be explained by the electrostatic attraction between polymer chains.

Figure 2.2e–g shows the phase diagrams that were prepared for a comprehensive understanding of the phase behavior. Three different parameters including polymer ratio, concentration of NaCl, and pH level were considered. First, the effects of pH level and NaCl concentration were investigated at a fixed polymer ratio (50 wt % PAA/50 wt % BPEI), as shown in **Figure 2.2e**. Only sol was observed, when the pH level was either below 2 or above 10. This could be explained by the deficiency in pairs of oppositely charged polymer chains to attract each other. At pH 2, PAA (pKa 4.5) tended to be uncharged, while amine groups of BPEI (pKa 4.5, 6.7, and 11.6) became almost charged. Finally, polymer chains remained dissolved in aqueous solutions with less electrostatic interaction. Meanwhile, only gel was observed at pH 4 regardless of NaCl concentration. This was probably due to sufficient oppositely charged groups of polymers such as COO^- (PAA), NH_3^+, NH_2^+, and NH^+ (BPEI), which could form physical cross–linking. These indicated that the pH levels were critical to determine the phase of the PAA/BPEI complexes. On the other hand, it was found that the addition of NaCl could lead to phase transition from gel to sol at pH 6 and 8. In addition, as the NaCl concentration increased, coacervate was observed in the way of a phase transition. This specified that, at the pH levels around neutral, NaCl could reduce the electrostatic interaction between PAA and BPEI. **Figure 2.4a** presents a lower rheological modulus of coacervate as the NaCl concentration increased, which was quantitative evidence of the effect of NaCl.

Next, the effect of the polymer ratio was studied at a fixed pH level of 6, as shown in **Figure 2.2f**. Regardless of polymer ratio, gel was obtained when NaCl was not added. This indicated that PAA/BPEI mixtures at pH 6 favored the formation of physical cross-linking. Regarding their pKa values, there could be a direct electrostatic attraction between polymer chains. In detail, the almost charged carboxylic acid of PAA (pKa 4.5) was able to combine with NH2 + and NH+ of BPEI (pKa 6.7 and 11.6) at pH 6. It was noted that almost all of the primary amine groups (pKa 4.5) on BPEI were less capable of participating in electrostatic binding with PAA because they favored the uncharged state (NH_2) at pH above 4.5. However, different phase behaviors, depending on the polymer ratio, were found as NaCl concentration increased. 0.7 M NaCl was sufficient to completely dissolve polymers in aqueous solution, when PAA was more than 90 wt %. On the other hand, at least 1.4 M was required for the complete disintegration of physical cross-linking, when PAA was less than 30 wt %. This implied that a large amount of charged amine groups of BPEI helped to form the gel. However, it was not definite that the electrostatic interaction was the major driving force for precipitation when PAA was less than 30 wt %. To be more specific, a larger amount of charged BPEI did not ensure stronger electrostatic binding between polymers. For example, at the same concentrations of NaCl of 1.4 and 2.1 M, sol was attained when PAA was less than 30 wt %, while coacervate was achieved when PAA was in the range of 50 to 70 wt %. Furthermore, the rheological modulus of coacervate at 0.7 M NaCl had the point of inflection as an increased ratio of PAA (**Figure 2.4c**). These results explained that the formation of gel at 0.7 M NaCl was not totally driven by the electrostatic interaction. This was probably due to the branched structure of PEI, which favored polymer agglomeration. As Li et al. previously claimed the effect of a branched structure on solidification,[22] this study confirmed it with the support of phase behavior and rheological analysis. Note that all complexes appeared to be sol at pH 6 regardless of the polymer ratio when the NaCl

concentration was more than 2.8 M. This was probably due to the reduction of entropy loss of binding and hydration at high salt conditions. In general, the shielding effect of salt was first considered in order to explain the electrostatic interaction. However, it became a minor factor, when the order of magnitude of salt concentration was too high.[32]

On the basis of the results of the phase study obtained from **Figure 2.2e, f**, an overall phase diagram at a fixed NaCl concentration of 0.7 M was prepared (**Figure 2.2g**). Similar to the results driven in **Figure 2.2e**, the phase strongly depended on the pH levels. In brief, sol was obtained when the conditions were extremely acidic or alkali, while gel could be formed when the polymer chains were exposed to the pH levels ranging from 3 to 6. In relation to coacervate, it was achieved near the neutral pH level, when PAA was in the range of 40 to 70 wt %. This indicated that an intermediate phase in the middle of the phase transition from gel to sol could be observed, when the pH level was controlled. In fact, a rheological feature of the coacervate could support the phase change from gel to sol as an increased pH level at a fixed polymer ratio. As shown in **Figure 2.4b**, when the pH level increased from 6 to 8, storage and loss modulus gradually decreased, which demonstrated a weaker electrostatic interaction between PAA and BPEI. This was certainly caused by the lower amount of charged amine groups (BPEI) capable of electrostatically binding to the fully charged carboxylic acid groups (PAA) at the elevated pH level. On the other hand, the effect of charged amine groups of BPEI on the formation of gel was also confirmed as well. At pH 6, an excess amount of BPEI helped to physically cross-link, which could be explained by the branched structure of BPEI, as similarly suggested in **Figure 2.2f**. This was also supported by the modulus analysis of coacervate, which had the point of inflection in both storage and loss modulus as an increased amount of BPEI at pH 6 (**Figure 2.4c**), which strongly implied that a larger amount of BPEI did not ensure a stronger electrostatic interaction between PAA and BPEI. To be more specific, the highest

rheological modulus could be acquired at an optimum polymer ratio at a fixed pH level. For example, the optimum polymer ratio was 60 and 50 wt % PAA at pH 6 and 8, respectively. This suggested that the ratio between oppositely charged polymers was essential to control electrostatic binding. In terms of stoichiometry, the result was reasonable, and this relationship could be extended to the gel, which influenced the adhesion strength of the physically cross-linked adhesives.

At last, each phase was quantitatively identified using complex viscosity calculated from the rheological modulus. This approach was quite practical, because complex viscosity expressed the total resistance to flow as a function of frequency. As a result, the gel showed an exceptional complex viscosity caused by the highest storage and loss modulus, as shown in **Figure 2.2h, i**. The range of complex viscosity of coacervate is also visually described in **Figure 2.2i**, which was calculated from the maximum and the minimum rheological modulus of coacervate (**Figure 2.2j**). For example, the complex viscosity of coacervate was in the range of 0.25 to 35 Pa·s at a fixed frequency of 1 s^{-1} , while the example of gel showed 300 Pa·s at the same frequency.

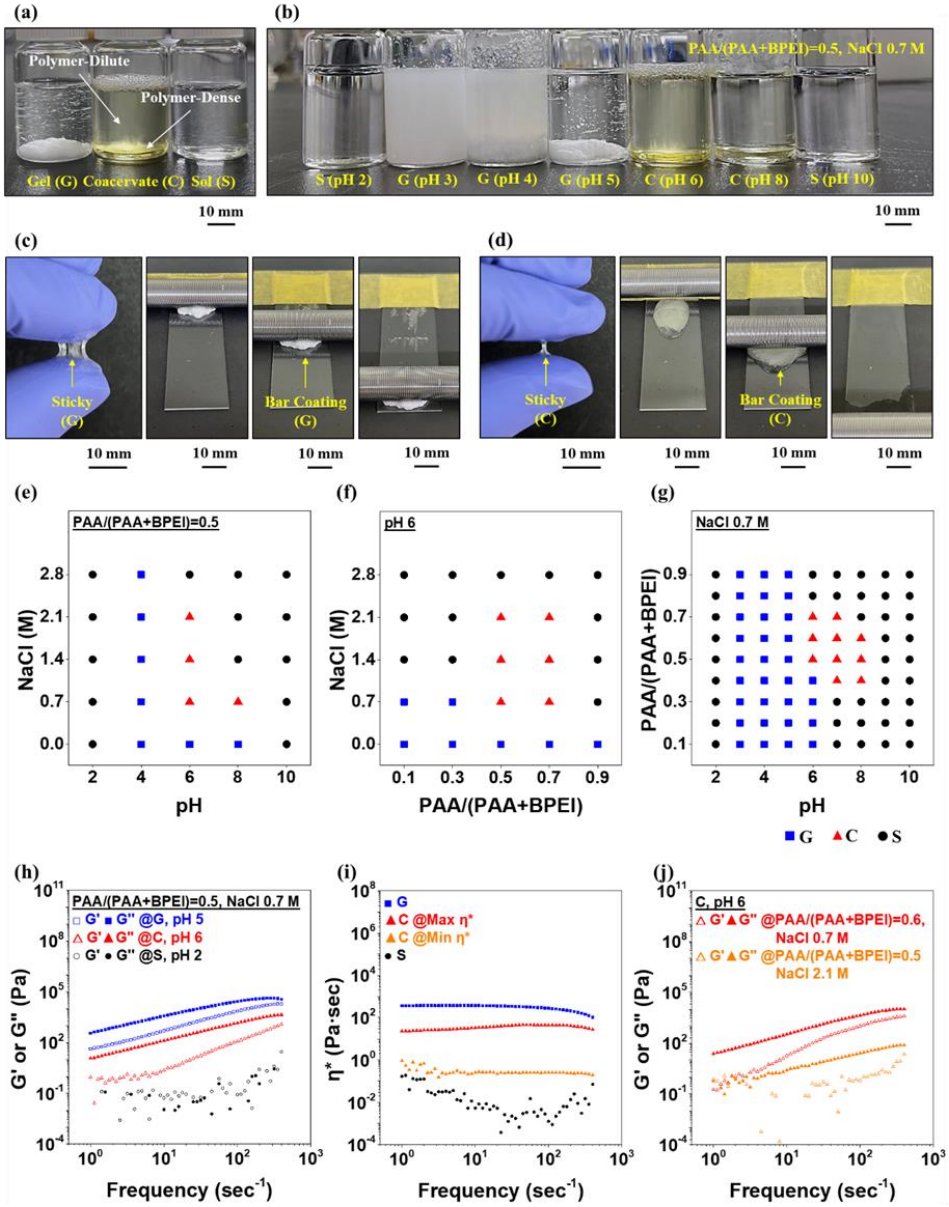

Figure 2.2. Phase study of PAA/BPEI complexes: (a) Three different phases of PAA/BPEI complexes. Coacervate was a polymer-dense region separated from a polymer-dilute region. (b) Phase study at different pH levels (PAA/(PAA+BPEI)=0.5, NaCl 0.7 M). (c) Non-uniform coating from a precipitated phase. (d) A coacervated phase could be facilely deposited on a glass substrate using the conventional Meyer rod method. (e) Phase diagram with different pH levels of varied concentration of NaCl. (f) Phase diagram with

different polymer ratios at varied concentration of NaCl. (g) Phase diagram with different pH levels at varied polymer ratios. (h) Rheology of PAA/BPEI complexes at different phases. (i) Rheological range of coacervates. Complex viscosity (η*) was calculated from the storage modulus (G'), loss modulus (G''), and frequency (ω), $\eta^* = \sqrt{(G'/\omega)^2 + (G''/\omega)^2}$. (j) Rheology of PAA/BPEI coacervates at different polymer ratios and different NaCl concentrations. Among the conditions of coacervates, red and orange result represents maximum and minimum viscosity, respectively.

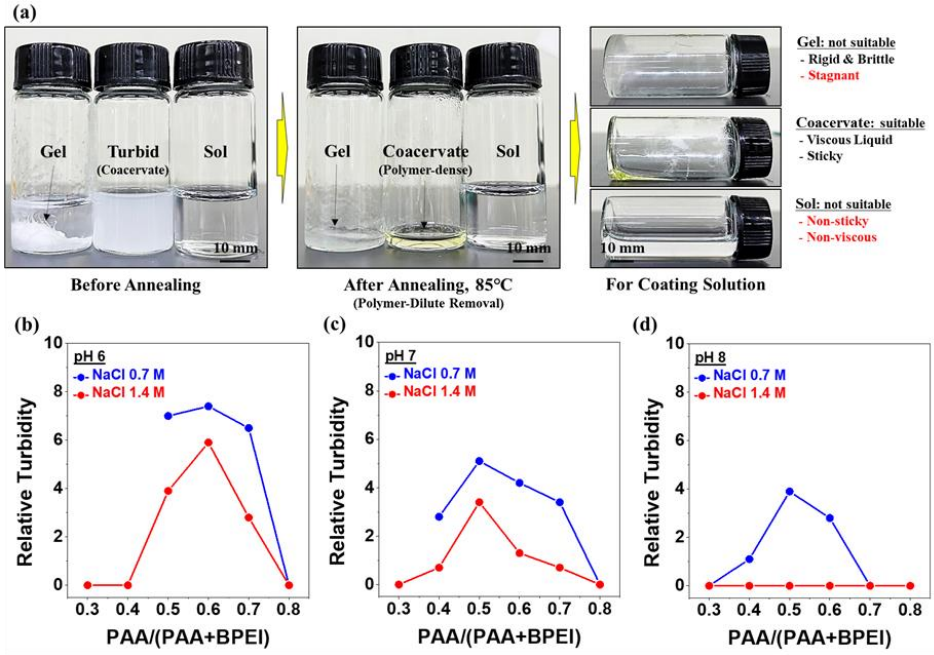

Figure 2.3. Phase identification and the relative turbidity: (a) Photos of each phase before and after the annealing process. Among three phases, coacervate was suitable for coating solution. Gel did not flow, while solution was not sticky. (b−d) The relative turbidity of turbid solution (pre−state of coacervate) and sol before annealing (b) at pH 6, (c) at pH 7, and (d) at pH 8. The relative turbidity of 0 indicated sol.

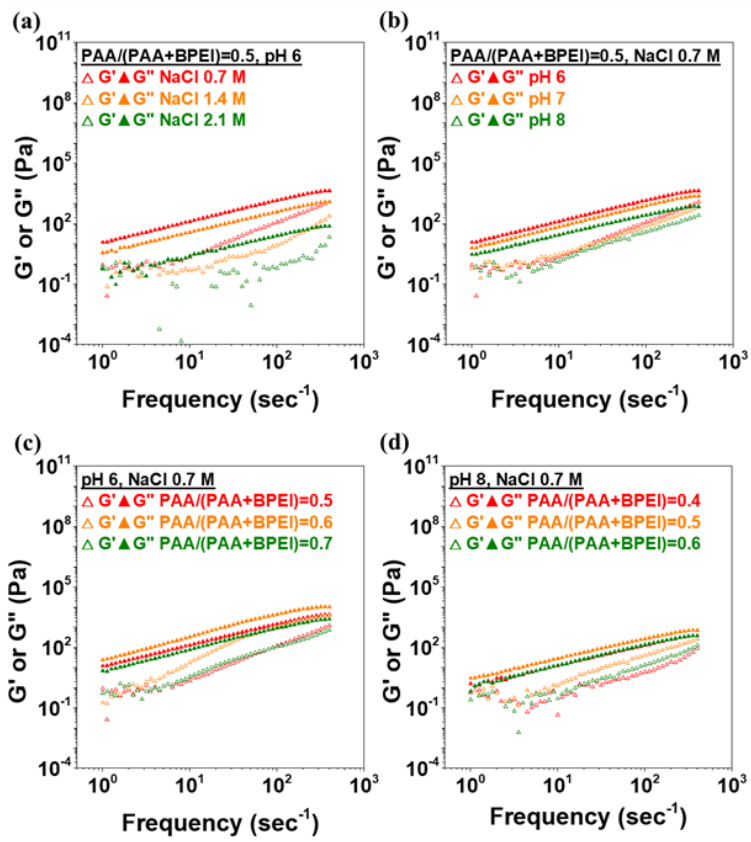

Figure 2.4. Rheology of PAA/BPEI coacervates: (a) Effect of the concentration of NaCl. (b) Effect of the pH level. (c) Effect of the polymer ratio at the fixed pH level of 6. (d) Effect of the polymer ratio at the fixed pH level of 8.

2.3.2. Adhesion properties of physically cross-linked PAA/BPEI complexes

To measure the adhesion strengths of physically cross-linked PAA/BEPI complexes, samples for the lap shear test should be prepared as described in **Figures 2.5a and 2.6a**. Here, coacervate was mainly used to load the adhesive layer, because other phases were not suitable for the rod coating method (**Figures 2.2c and 2.3a**). Also, the turbid solution, the prestate of coacervate, seemed to have a lower density of charged colloids, because adhesion performance was significantly poor (~0 kPa). A lap shear joint was fixed at 20 mm × 10 mm, and the adhesive area was pressed with a 20 g weight for 2 h at RT. In particular, the pH-induced phase transition from the coacervate to gel was applied for the formation of gel adhesive. For example, substrate was dipped into a 1 M citrate aqueous buffer solution of pH 5 after coacervate (60 wt % PAA, pH 6, 0.7 M NaCl) deposition. Then, coacervate started to solidify and became opaque, which resulted in a gel layer (60 wt % PAA, pH 5, 0.7 M NaCl) in 30 s. This simple and uniform coating process was accomplished by the conventional rod coating method using fluidic coacervate, as described in **Figure 2.2d**. Thus, physically cross-linked adhesive layers could be systemically deposited on corona-treated PET films. Furthermore, it took less than 1 min including the phase transition to load the gel layer. This suggested that coacervate could potentially be regarded as a polyelectrolyte coating solution, because this material did not require multiple steps for electrostatic binding between oppositely charged polymers, like layer-by-layer assembly. In addition, a reverse phase transition from gel to coacervate was also possible, so that a recyclable adhesive system could be expected. For example, a gel prepared at pH 5 could become a coacervate through the dissolution process at an elevated pH level (pH 8, tris-buffer solution).

The adhesion strengths of the coacervates with different parameters such as polymer ratio, concentration of NaCl, and pH level were evaluated. **Figure 2.5b-d** shows the stress- displacement

curves obtained from the lap shear test with the crosshead speed of 10 mm/min. The adhesion strength tended to become weaker as the amount of NaCl increased (**Figure 2.5b**) or the pH level elevated (**Figure 2.5c**). Considering the rheological properties studied in Section 2.3.1, more intensive load was required to break the highly viscous coacervate adhesive. **Figure 2.5d** describes an optimum polymer ratio (60 wt % PAA/40 wt % BPEI) at a given condition (pH 6, 0.7 M NaCl). As demonstrated in the inset photo, coacervate was able to endure up to 20 kPa (200 g/cm^2). In fact, the optimum polymer ratio varied, depending on the pH level. This was because charges of the amine groups (BPEI) were strictly determined by the concentration of proton in the aqueous solution. For example, the increased pH level from 6 to 8 demanded more weight of BPEI from 40 to 50 wt % in order to compensate for the lesser charged amine groups (**Figure 2.5e**). The rheological moduli shown in **Figure 2.4c, d** supported this trend in terms of electrostatic interaction, and it also considerably coincided with the relative turbidity discussed in **Figure 2.3b**. Nevertheless, it is reasonable to regard the pH level as the leading factor to determine the adhesion strength of the coacervate, because an increased ratio of BPEI was not able to overcome the drop of adhesion strength when the pH level was elevated.

Next, lap shear tests of gels at different polymer ratios and pH levels were performed, as shown in **Figure 2.6b–d**. Here, the pH level was defined on the basis of the citrate buffer solution used for the phase transition. The NaCl concentration was fixed at 0.7 M, because an excess amount of NaCl caused a significant drop of adhesion strength, as demonstrated in **Figure 2.7b**. As expected, the formation of gel by pH–induced phase transition contributed to improved adhesion strength. For example, a 50% increase in adhesion strength was achieved by solidification at pH 5, compared to coacervate at pH 6 when PAA was 60 wt %. This led to an adhesion strength of 30 kPa (300 g/cm^2) (**Figure 2.6b**). Except for a few catechol–based glues such as polydopamine[37] and tannic acid,[38] this value was strong enough to compete with several hydrogel–based adhesives (**Table**

2.1).[15–17,33–41] In fact, the optimum pH level where the maximum adhesion strength of the gel was obtained depended on the polymer ratio, as confirmed in **Figure 2.6e**. To be more detailed, the increased ratio of PAA from 60 to 70 wt % released more unreacted charged carboxylic acid groups. Then, more acidic solution was demanded to compensate for the lower amount of charged amine groups (BPEI). As a result, the pH level should be controlled from 5 to 4 in an attempt to provide more charged amine groups, NH_3^+. However, solidification did not always ensure enhanced adhesion strength, compared to coacervate. For example, solidification at pH 3 led to a decrease in adhesion strength, compared to coacervate at pH 6, as shown in **Figure 2.6b, c**. In terms of electrostatic interaction, weak binding between PAA and BPEI could be one reason, in that carboxylic acid groups (PAA) favorably became uncharged at pH 3. Even though solidification occurred at a given pH level, this seemed to be driven by agglomeration caused by the branched structure of PEI. As discussed in **Figure 2.2b**, different shapes of gels indirectly support a decrease in electrostatic attraction at pH 3, compared to pH 5. Similarly, BPEI–rich gel did not effectively improve adhesion strength, as presented in **Figure 2.6d**. This was probably due to the unbalanced stoichiometry between oppositely charged polymers. Also, a weak electrostatic binding of BPEI–rich polymer complexes could be another cause, as implied in **Figure 2.2f**. However, these cases such as solidification at pH 3 and BPEI–rich gel were not clearly understood, because lap shear adhesion strength was also determined by how solid it was. For example, a too brittle adhesive layer could negatively affect adhesion strength.

Figure 2.8 demonstrates the repeatable adhesion properties of coacervate and gel. This was attributed to physically cross–linked polymers, so that the detached surface could be reversibly recovered. Here, a drop of citrate buffer solution (100 mL/m^2) was applied on the detached surface to accelerate the recovery rate by enhancing the mobility of the polymer chains. In detail, a citrate buffer solution of pH 6 and 5 was used on the coacervate and gel, respectively

(**Figure 2.8a**). Then, scratches disappeared in 30 min with complete reattachment, as described in **Figure 2.8b**. **Figure 2.8c, d** shows the repeatable adhesion properties during the cyclic attachment/ detachment tests. At least 80% of the initial adhesion strength was found to be retained during 5 adhesion cycles. This adhesion efficiency was comparable to the direct fabricated gel adhesive, which indicated that the pH−induced phase transition method worked well. As reported by Zhang et al., an adhesion efficiency on the hydrogel substrate was 60− 87 % during 5 adhesion cycles, when the gel adhesive was directly fabricated without the control of pH level as well as the amount of salt.[16]

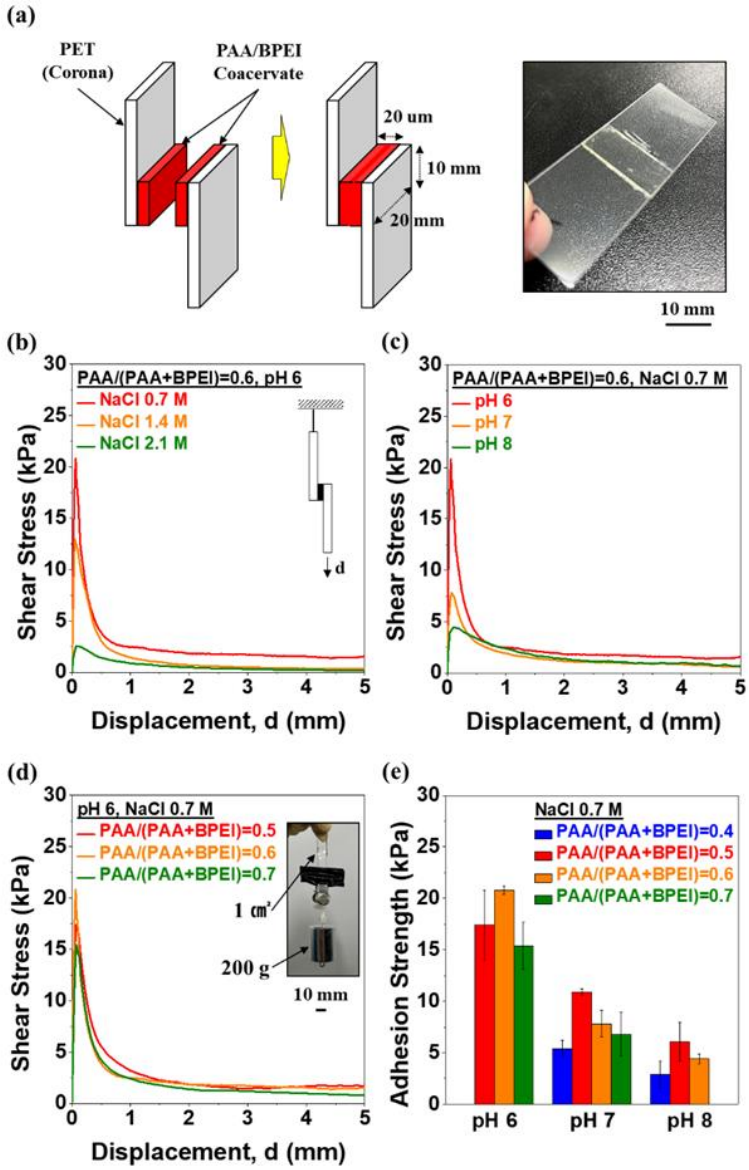

Figure 2.5. Adhesion properties of PAA/BPEI coacervates: (a) Schematic and photo of sample preparation for the lap shear test. (b) Stress-displacement curves of coacervates at different concentrations of NaCl. (c) Stress-displacement curves at different pH levels. (d) Stress-displacement curves at different ratios of polymers. Inset demonstrates the adhesion strength of 20 kPa (200 g/cm^2) (e) Adhesion strength of the PAA/BPEI coacervates.

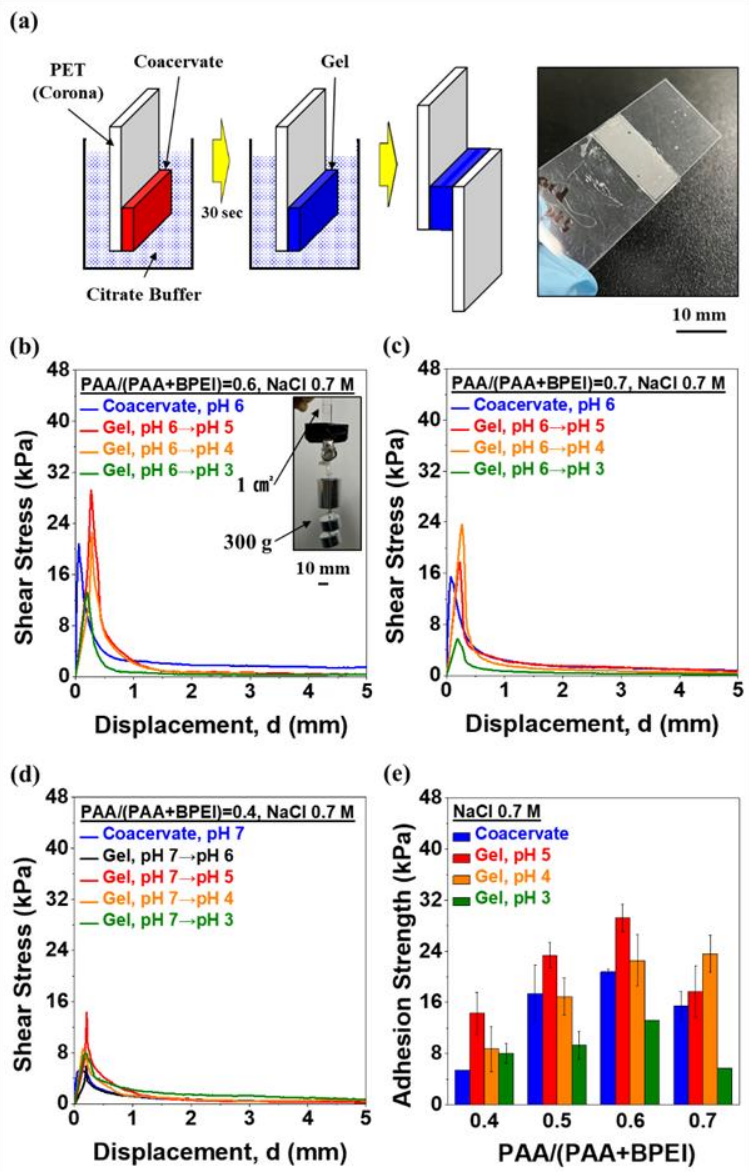

Figure 2.6. Adhesion properties of PAA/BPEI gels: (a) Schematic and photo of sample preparation for the lap shear test. Gel adhesive could be fabricated by pH-induced phase transition. (b) Stress-displacement curves of gels (PAA/(PAA+BPEI)=0.6) at different pH levels. Inset demonstrates the adhesion strength of 30 kPa (300 g/cm^2). (c) Stress-displacement curves of gels (PAA/(PAA+BPEI)=0.7) at different pH levels. (d) Stress-displacement curves of gels (PAA/(PAA+BPEI)=0.4) at different pH levels. (e) Adhesion

strength of PAA/BPEI gels. All the pH values for coacervates was 6, except coacervate of PAA/(PAA+BPEI)=0.4 that was formed at pH 7.

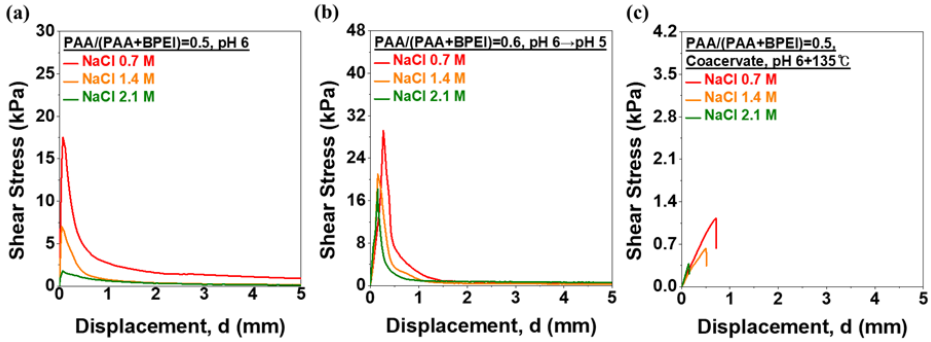

Figure 2.7. Stress-displacement curves of PAA/BPEI complexes: (a) Effect of the concentration of NaCl on the adhesion strength of coacervate. (b) Effect of the concentration of NaCl on the adhesion strength of gel. (c) Effect of the concentration of NaCl on the adhesion strength of thermally treated coacervate.

Ref. (SI)	Material	Adhesion Strength (kPa)					Note.
		*Plastic	Glass	Rubber	**Metal	Skin	
15 (1)	PDADMAC/P(AAm-AAc)	7.3	7.8	4.3	6.4	6.3	
17 (2)	PDDA/Folic Acid	33	139		167		
33 (3)	PVA/PSBMA	7.6	6.1	7.7	6.8	7.2	
34 (4)	Gelatin/Tannic Acid	21	17	14	30		
35 (5)	PAA/Tannic Acid		35		45	26	
36 (6)	PAA/Pectin/Lignin		38		50	28	
37 (7)	PDA/PAM	81	120		81	29	
38 (8)	PHEAA/Tannic Acid	522	322		722		
39 (9)	PEG	29	58		56	76	
40 (10)	PAM	12	50		35		
41 (11)	PAM	22	29		43	34	
42 (12)	3M	320	2.3 MPa	75	300		Product
43 (13)	3M		900		1.6 MPa		Product
43	Loctite		1.4 MPa		2.0 MPa		Product
43	Lubrizol		900		2.9 MPa		Product
This Work	PAA/BPEI (Coacervate)	20	35	10			
	PAA/BPEI (Phase Transition)	30	61	15			
	PAA/BPEI-Amide (Thermal Treatment)	2.4 MPa	3.3 MPa	44			

*PE, PET, PP, PMMA, PVC, PVA **Al, Ti, Fe, Cu

Table 2.1. Reported adhesion strength of hydrogel.

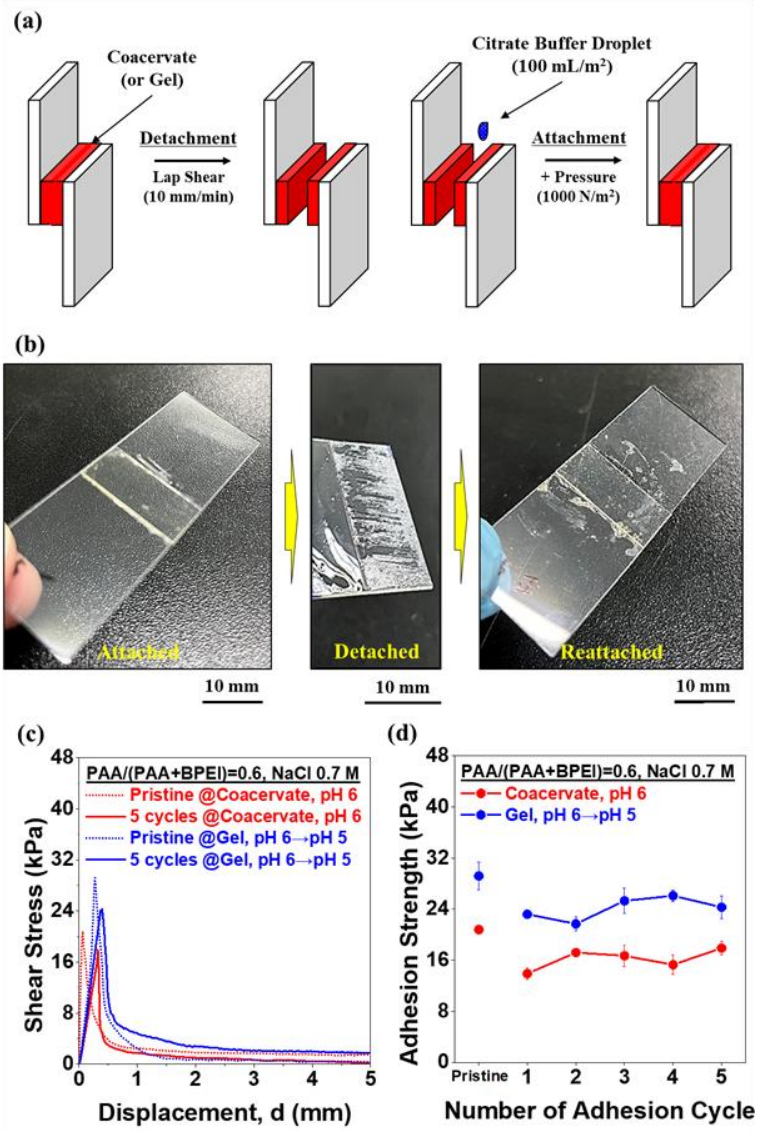

Figure 2.8. Repeatable adhesion of PAA/BPEI complexes: (a) Schematic of repeatable adhesion test. A drop of citrate buffer solution applied to the detached surface helped to accelerate the rate of recovery, so that adhesive could be recovered in 30 min. (b) Photos of repeatable adhesive. Scratches on the detached surface disappeared, when reattached. (c) Stress-displacement curve of coacervate (PAA/(PAA+BPEI)=0.6, pH 6, NaCl 0.7 M) and gel (pH 5) after 5 cycles. (d) Adhesion strength of coacervate (PAA/(PAA+BPEI)=0.6, NaCl 0.7 M) and gel (pH 5) during cyclic

attachment/detachment tests. More than 80 % of the initial adhesion strength was retained after 5 adhesion cycles.

2.3.3. Adhesion properties of thermally treated PAA/BPEI complexes

Stronger adhesion strength could be achieved through the formation of a chemical linkage within the gels. The reaction of carboxylic acid with amine would be expected to form an amide linkage. As described in **Figure 2.9a**, this conversion required a temperature above 100 °C for water driven off to hinder a reverse reaction. On the basis of this mechanism, the formation of amide linkage was acquired when the PAA/BPEI gel was heated at 135 °C, and FTIR analysis demonstrated it. As shown in **Figure 2.9b** (orange), the peak at 1310 cm^{-1} (C=O stretch, carboxylic acid) almost disappeared with a slightly increased intensity at 1660 cm^{-1} (C=O stretch, amide). This indicated that the carboxylic acid of PAA became engaged in the chemical reaction for the formation of an amide linkage. However, this chemical reaction seemed to barely occur when PAA/BPEI coacervate was heated (red). This was probably due to fewer amounts of electrostatic pairs and low mobility of the polymer chains caused by water being driven off.

Next, **Figure 2.9c, d** shows the stress–displacement curves of the lap shear tests of thermally treated PAA/BPEI at a fixed NaCl concentration of 0.7 M. All samples were stabilized in the chamber at a relative humidity of 90% RH at 40 °C for 24 h before the measurements. Then, **Figure 2.9e** summarizes the adhesion strengths of the PAA/BPEI complexes, which showed a dramatically enhanced adhesion strength by thermal treatment. For example, adhesion strength was increased by 100 times from 24 kPa to 2.4 MPa, when PAA was 50 wt %. This was probably due to the reinforced fracture strength of the adhesive layer by the formation of chemical bonding. In fact, this adhesive layer could be regarded as gel, because it tended to uptake water. The equilibrium swelling ratio of the gel (50 wt% PAA, pH 5, 0.7 M NaCl) at a relative humidity of 90% RH was about 28 wt % (**Figure 2.10**). This was probably due to the hydrophilic characteristics of the amide linkage and unreacted functional groups that were capable of attracting water. On the other

hand, a lower effect on adhesion strength enhancement was confirmed when coacervate was thermally treated, as seen in **Figure 2.9c**. For example, adhesion strength was increased by 69 times from 17.5 kPa to 1.2 MPa when PAA was 50 wt %. This result was identical with FTIR analysis discussed in **Figure 2.9b**, in that lower amounts of amide linkage were formed when coacervate was heated. Also, the swelling ratio of thermally treated coacervate (56 wt %) was 2 times higher than that of the thermally treated gel at a relative humidity of 90 % RH (**Figure 2.10**), which revealed that the higher water content was caused by unreacted functional groups. In terms of NaCl, it was also reasonable that an increased amount of NaCl impacted both adhesion strength and swelling ratio when thermally treated. An example of thermally treated coacervate (50 wt % PAA) showed that the adhesion strength decreased from 1.2 to 0.4 MPa with an increased swelling ratio from 56 to 121 wt % when the NaCl concentration changed from 0.7 to 2.1 M (**Figures 2.7c and 2.10**). This was possibly related to the shielding effect and entropy loss by NaCl. Briefly, a sufficient amount of the chemical reaction between carboxylic acid and amine was hindered, because each polymer chain tended to be distributed with less electrostatic interaction as the amount of NaCl increased. Meanwhile, stoichiometry between PAA and BPEI should be controlled to achieve the utmost enhancement of adhesion strength. This could be explained by the ratio between carboxylic acid and amine potentially engaged in the formation of an amide linkage. In this polymer system, a controlled ratio of PAA of around 50 wt% was recommended for the adhesion strength of a commercial product. Zhang et al. and Cui et al. reported the result of the lap shear test of 3M and Loctite on a glass substrate of about 2.3 and 1.4 MPa, respectively (**Table 2.1**).[42,43]

Lastly, we evaluated underwater adhesion strength using thermally treated gel adhesive (50 wt % PAA, pH 5, 0.7 M NaCl). It could endure in a water bath without detachment, while both coacervate and gel without thermal treatment lost their adhesion properties under water. However, underwater adhesion strength was

significantly decreased from 2.4 MPa to 450 kPa (**Figure 2.11**). Even though a drop of adhesion strength occurred, it could reach the level of commercial products considering the lap shear result of 3M and Loctite on the metal substrate of about 300 and 500 kPa, respectively.[44]

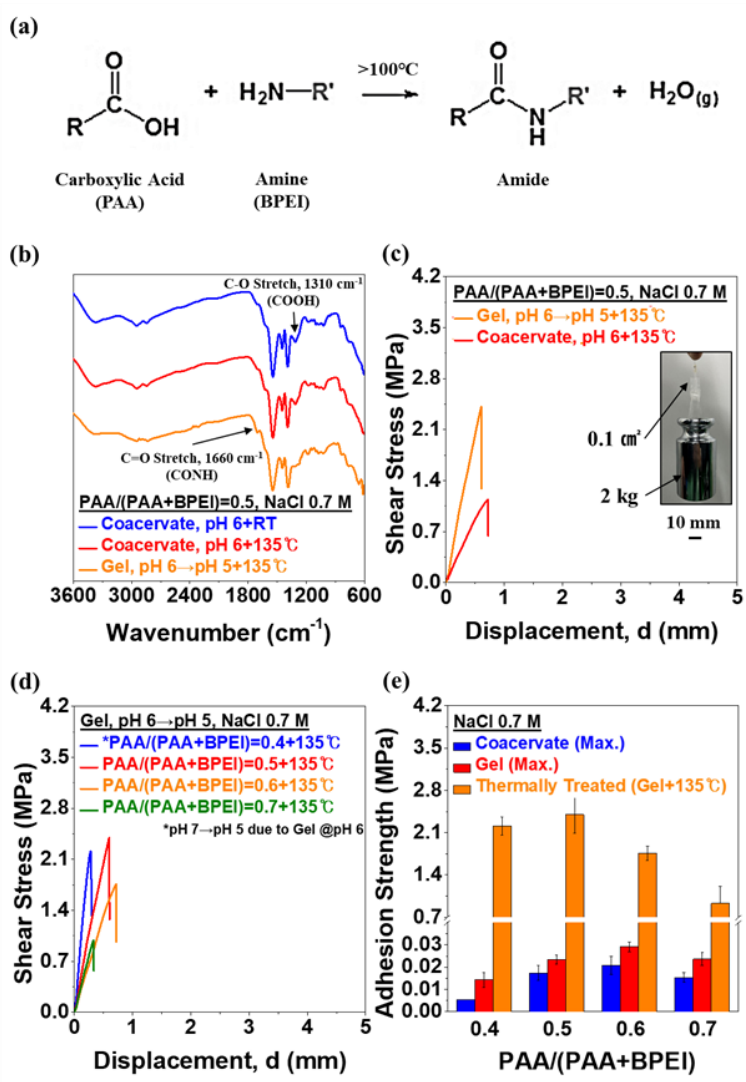

Figure 2.9. Thermal treatment of PAA/BPEI Adhesives: (a) Chemical reaction of carboxylic acid (PAA) and amine (BPEI) to form amide bonding. A temperature above 100 °C is required for water to be driven off. (b) FTIR spectra showing the formation of amide linkage, when gels were heated at 135 °C. (c) Stress-displacement curves of PAA/BPEI after heating at different phases. Inset demonstrated the adhesion strength of 2 MPa (20 kg/cm^2). (d) Stress-displacement curves of PAA/BPEI after heating at different polymer ratios of gels. (e) Adhesion strength after thermal treatment.

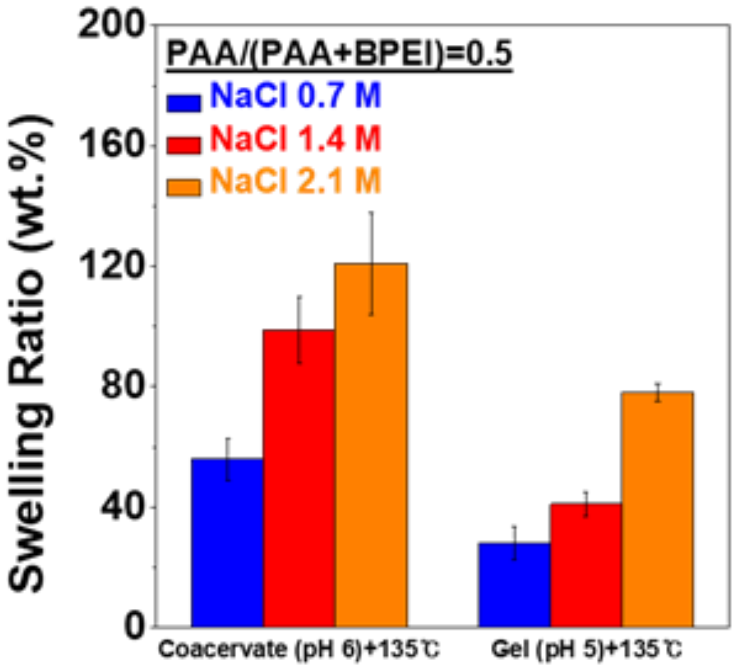

Figure 2.10. Swelling ratio of thermally treated coacervate and gel with respect to the concentration of NaCl.

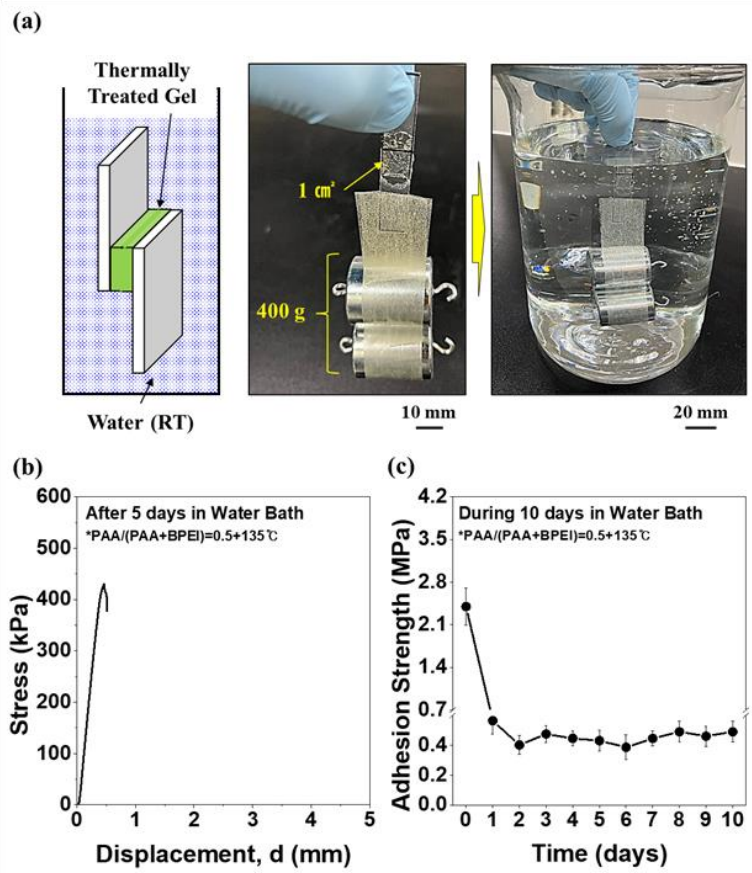

Figure 2.11. Underwater adhesion of thermally treated gel: (a) Schematic and photos of underwater adhesion test (b) Stress-displacement curve of thermally treated gel (PAA/(PAA+BPEI)=0.5) after 5 days in water bath. (c) Underwater adhesion strength of thermally treated gel during 10 days.

2.3.4. Adhesion properties of PAA/BPEI complexes on several substrates

The adhesion strengths of the PAA/BPEI complexes were compared under several substrate conditions. Three different substrates of PET film, glass, and rubber sheet were prepared. Then, each substrate was further treated by corona discharge to reduce the contact angle for the wettability of coacervate (**Figure 2.12m**). **Figure 2.12a–c** presents the results of the lap shear tests by substrate conditions, while **Figure 2.12d–g** captures typical fracture images. Regardless of the type of adhesive, corona–treated glass shows the strongest adhesion strength. For example, gel adhesive could endure up to 61 kPa, and thermally treated adhesive did not disintegrate until 3.3 MPa was loaded. Furthermore, glass tended to show enhanced adhesive performance, compared to the PET film. On the other hand, 15 kPa at most was enough to disintegrate the rubber sheets attached by the gel. Also, low adhesion strength (<45 kPa) was measured, even though the gel adhesive was thermally treated. **Figure 2.12g** visually shows a little amount of residue on the corona–treated rubber sheet after detachment, which indicates poor adhesion, compared to the PET film as well as glass (**Figure 2.12d–f**). This probably resulted from the hydrophobicity of rubber material, which contributed to the degradation of wettability and adhesion of PAA/BPEI complexes. As shown in **Figures 2.12l and 2.13**, the contact angles of the adhesives were at most 22 °, while that of the rubber sheet was about 104 ° (**Figures 2.12m and 2.14**). Further, we presumed the rough surface of the rubber sheet hindered the penetration of the coacervate, because the adhesion strength of the corona–treated rubber sheet (contact angle of 63 °) was still significantly degraded. **Figure 2.12n** shows the higher surface roughness of the rubber sheet, and **Figure 2.12k** visually supports the unevenness of the surface, compared to the other substrates (**Figure 2.12h–j**). Note that the rough surface of the rubber sheet was not generated by the corona discharge (**Figures 2.12n and 2.15**). This suggested the mechanism was almost consistent with the

previous work by Zhao et al., which reported wetting failure could be promoted by roughness, even on hydrophilic surfaces.[45] On the other hand, it was also necessary to consider the reason; when thermally treated adhesive was applied on the bare PET film, it did not work sufficiently. This was believed to be because the amine of the coacervate could chemically react with hydrophilic functional groups such as phenolics, aldehydes, and esters on the corona-treated PET film, while there were less reactive functional groups on the bare PET film.[46,47] **Figure 2.12d** shows a larger area of interfacial fracture, compared to **Figure 2.12e**, which implies a lower amount of chemical bonding between the adhesive components and the bare PET film.

In fact, a more in-depth and explicit study on the adhesion mechanism is still required, because there were some cases that contrasted with the trend. In particular, it was ambiguous to analyze adhesion when the contact angle was less than 90 °, which indicated good wetting. For example, the adhesion strength of bare glass was much stronger than that of the corona-treated PET film. This was not rational, because the contact angle of the corona-treated PET film was smaller than that of the bare glass. We thought that hydrophilic polymers such as PAA and BPEI could not physically interact with the hydrophobic bulk adherend like PET, even though the corona discharge made the surface hydrophilic.

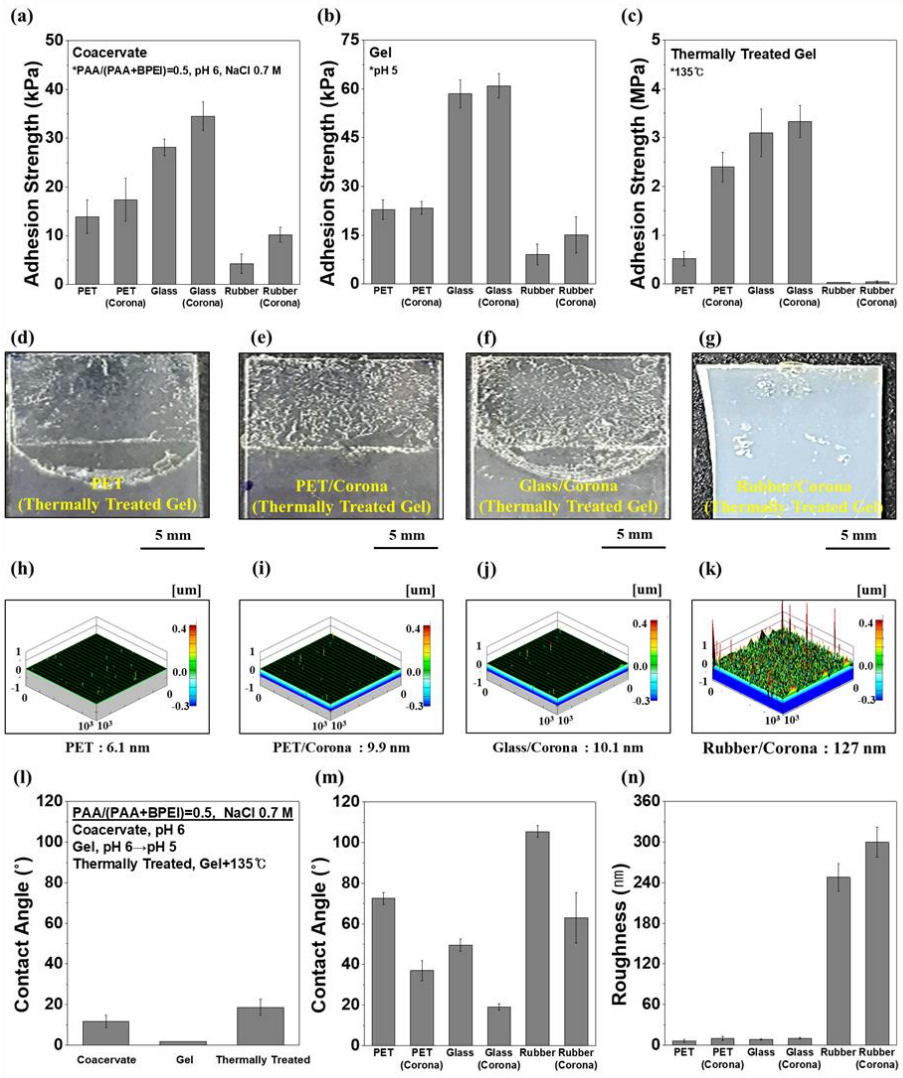

Figure 2.12. Adhesion properties of PAA/BPEI on various substrates: (a) Adhesion strength of coacervates on different substrates. (b) Adhesion strength of gels on different substrates. (c) Adhesion strength of thermally treated gels on different substrates. (d–g) Residue of thermally treated gels after the detachment (d) on PET, (e) on corona–treated PET, (f) on corona–treated glass, and (g) on corona–treated rubber. (h–k) Surface roughness (h) of PET, (i) of corona–treated PET, (j) of corona–treated glass, and (k) of corona–treated rubber. (l) Contact angle measurements of PAA/BPEI

adhesives. (m) Contact angle measurements of substrates. (n) Surface roughness measurements of substrates.

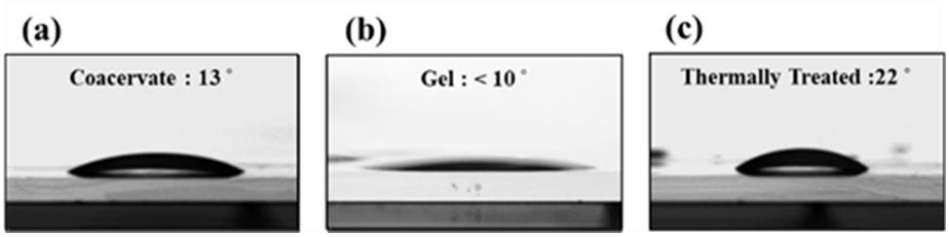

Figure 2.13. Contact angle measurements of PAA/BPEI complexes deposited on glass, where PAA/(PAA+BPEI)=0.5 and NaCl 0.7 M: (a) Coacervate, (b) Gel, and (c) Thermally treated adhesive.

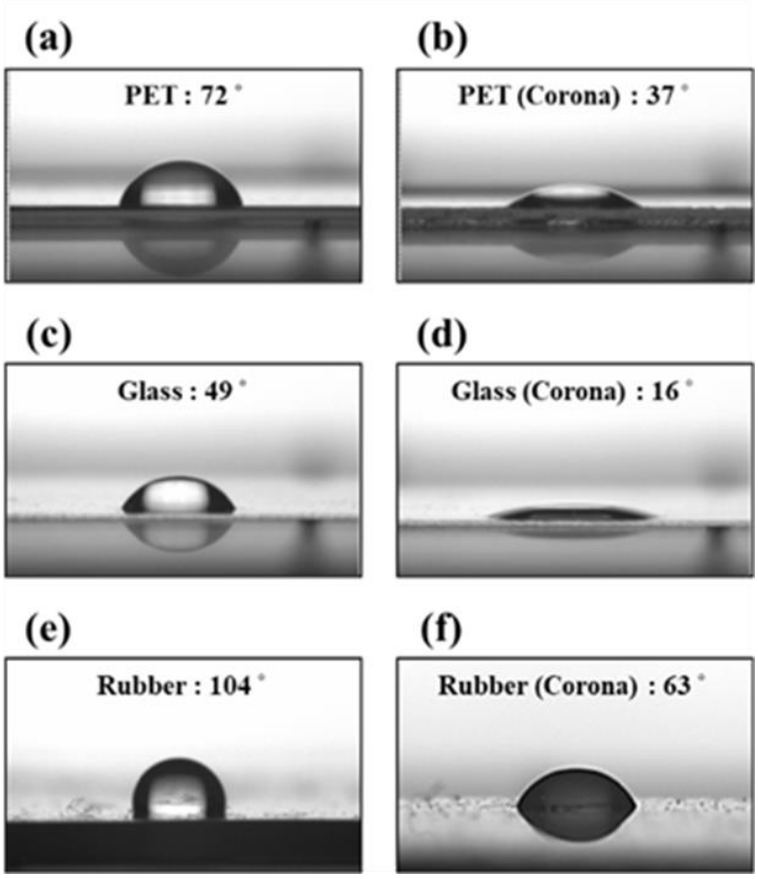

Figure 2.14. Contact angle measurements of substrates: (a) PET film, (b) Corona-treated PET film, (c) Glass, (d) Corona-treated glass, (e) Rubber sheet, and (f) Corona-treated rubber sheet.

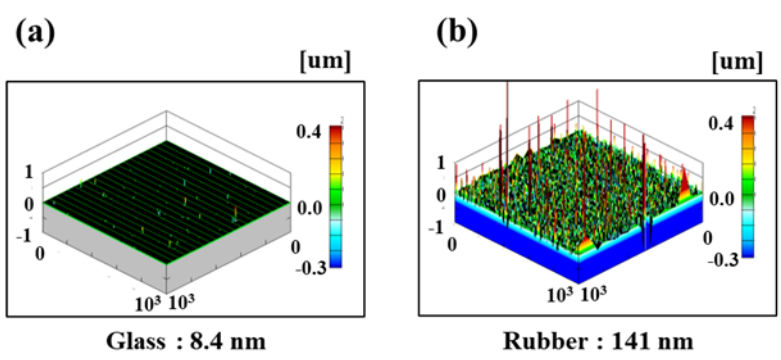

Figure 2.15. Surface roughness measurements of substrates: (a) Glass, and (b) Rubber sheet.

2.4. Conclusion

PAA/BPEI complexes have three different phases of gel, coacervate, and sol, which were determined by parameters that included the polymer ratio, concentration of NaCl, and pH level. Briefly, these three parameters controlled the electrostatic interaction between oppositely charged polymers, so that the phase as well as the rheological characteristics were changed. Fluidic coacervate was suitable for a polyelectrolyte coating solution, and the gel layer could be facilely loaded using a pH-induced phase transition. In relation to polyelectrolyte adhesives, it was found that a higher viscous phase led to more intensive adhesion strength. In addition, thermal treatment helped to obtain a dramatic increase in adhesion strength (2.4 MPa, corona-treated PET film), which was accomplished by conversion from carboxylic acid to amide. However, hydrophobic or rough surfaces seemed to result in the deterioration of phase transitional polyelectrolyte adhesives. For example, rubber sheets did not join well regardless of the corona discharge. Even though a more in-depth study on the adhesion mechanism is required, we expect that the coacervate coating system could potentially be applicable to the polyelectrolyte deposition fields including adhesives, actuators, and barriers.

Reference

(1) Prescher, S.; Polzer, F.; Yang, Y.; Siebenbu¨rger, M.; Ballauff, M.; Yuan, J. Polyelectrolyte as Solvent and Reaction Medium. J. Am. Chem. Soc. 2014, 136, 12−15.

(2) Wang, Q.; Schlenoff, J. B. Single− and Multicompartment Hollow Polyelectrolyte Complex Microcapsules by One−Step Spraying. Adv. Mater. 2015, 27, 2077−2082.

(3) Zhao, J.; Chen, Y.; Yao, Y.; Tong, Z.−R.; Li, P.−W.; Yang, Z.−M.; Jin, S.−H. Preparation of the Polyelectrolyte Complex Hydrogel of Biopolymers via a Semi−Dissolution Acidification Sol−Gel Transition Method and its Application in Solid−State Supercapacitors. J. Power Sources 2018, 378, 603−609.

(4) Zhang, W.; Zhao, Q.; Yuan, J. Porous Polyelectrolytes: The Interplay of Charge Pores for More Functionalities. Angew. Chem., Int. Ed. 2018, 57, 6754−6773.

(5) Potaufeux, J.−E.; Odent, J.; Notta−Cuvier, D.; Lauro, F.; Raquez, J.− M. A Comprehensive Review of the Structures and Properties of Ionic Polymeric Materials. Polym. Chem. 2020, 11, 5914−5936.

(6) Li, X.; Liu, C.; Van der Bruggen, B. Polyelectrolytes Self−Assembly: Versatile Membrane Fabrication Strategy. J. Mater. Chem. A 2020, 8, 20870−20896.

(7) Slyusareva, E.; Gerasimova, M.; Plotnikov, A.; Sizykh, A. Spectral Study of Fluorone Dyes Adsorption on Chitosan−Based Polyelectrolyte Complexes. J. Colloid Interface Sci. 2014, 417, 80−87.

(8) Wang, D.; Gong, X.; Heeger, P. S.; Rininsland, F.; Bazan, G. C.;

Heeger, A. J. Biosensors from Conjugated Polyelectrolyte Complexes. Proc. Natl. Acad. Sci. U.S.A. 2002, 99, 49−53.

(9) Mei, X.; Ye, D.; Zhang, F.; Di, C.−A. Implantable Application of Polymer−Based Biosensors. J. Polym. Sci. 2022, 60, 328−347.

(10) Song, Y.; Qin, S.; Gerringer, J.; Grunlan, J. C. Unusually Fast and Large Actuation from Multilayer Polyelectrolyte Thin Films. Soft Matter 2019, 15, 2311−2314.

(11) Glazer, P. J.; van Erp, M.; Embrechts, A.; Lemay, S. G.; Mendes, E. Role of pH Gradients in the Actuation of Electro−Responsive Polyelectrolyte Gels. Soft Matter 2012, 8, 4421−4426.

(12) Li, C.; Gu, Y.; Zacharia, N. S. Tuning Wet Adhesion of Weak Polyelectrolyte Multilayers. ACS Appl. Mater. Interfaces 2018, 10, 7401−7412.

(13) Manoj Lalwani, S.; Eneh, C. I.; Lutkenhaus, J. L. Emerging Trends in the Dynamics of Polyelectrolyte Complexes. Phys. Chem. Chem. Phys. 2020, 22, 24157−24177.

(14) Alfhaid, L.; Williams, N. H.; Geoghegan, M. Adhesion between Oppositely Charged Polyelectrolytes in Salt Solution. J. Appl. Polym. Sci. 2020, 137, 49130.

(15) Li, W.; Feng, R.; Wang, R.; Li, D.; Jiang, W.; Liu, H.; Guo, Z.; Serpe, M. J.; Hu, L. Polyelectrolyte−Based Physical Adhesive Hydrogels with Excellent Mechanical Properties for Biomedical Applications. J. Mater. Chem. B 2018, 6, 4799−4807.

(16) Zhang, J.−N.; Zhu, H.; Liu, T.; Chen, Y.; Jiao, C.; He, C.; Wang, H. Strong Adhesion of Hydrogels by Polyelectrolyte Adhesives. Polymer 2020, 206, 122845.

(17) Gao, S.; Wang, W.; Wu, T.; Jiang, S.; Qi, J.; Zhu, Z.; Zhang, B.; Huang, J.; Yan, Y. Folic Acid-Based Coacervate Leading to a Double-Sided Tape for Adhesion of Diverse Wet and Dry Substrates. ACS Appl. Mater. Interfaces 2021, 13, 34843-34850.

(18) Wang, Q.; Schlenoff, J. B. The Polyelectrolyte Complex/ Coacervate Continuum. Macromolecules 2014, 47, 3108-3116.

(19) Chollakup, R.; Beck, J. B.; Dirnberger, K.; Tirrell, M.; Eisenbach, C. D. Polyelectrolyte Molecular Weight and Salt Effects on the Phase Behavior and Coacervation of Aqueous Solutions of Poly(acrylic acid) Sodium Salt and Poly(allylamine) Hydrochloride. Macromolecules 2013, 46, 2376-2390.

(20) Wang, J.; Cohen Stuart, M. A.; van der Gucht, J. Phase Diagram of Coacervate Complexes Containing Reversible Coordination Structures. Macromolecules 2012, 45, 8903-8909.

(21) Danielsen, S. P. O.; Nguyen, T.-Q.; Fredrickson, G. H.; Segalman, R. A. Complexation of a Conjugated Polyelectrolyte and Impact on Optoelectronic Properties. ACS Macro Lett. 2019, 8, 88-94.

(22) Li, J.; van Ewijk, G.; van Dijken, D. J.; van der Gucht, J.; de Vos, W. M. Single-Step Application of Polyelectrolyte Complex Films as Oxygen Barrier Coatings. ACS Appl. Mater. Interfaces 2021, 13, 21844- 21853.

(23) Haile, M.; Sarwar, O.; Henderson, R.; Smith, R.; Grunlan, J. C. Polyelectrolyte Coacervates Deposited as High Gas Barrier Thin Films. Macromol. Rapid Commun. 2017, 38, 1600594.

(24) Smith, R. J.; Long, C. T.; Grunlan, J. C. Transparent

Polyelectrolyte Complex Thin Films with Ultralow Oxygen Transmission Rate. Langmuir 2018, 34, 11086−11091.

(25) Kelly, K. D.; Schlenoff, J. B. Spin−Coated Polyelectrolyte Coacervate Films. ACS Appl. Mater. Interfaces 2015, 7, 13980−13986.

(26) Kurtz, I. S.; Sui, S.; Hao, X.; Huang, M.; Perry, S. L.; Schiffman, J. D. Bacteria−Resistant, Transparent, Free−Standing Films Prepared from Complex Coacervates. ACS Appl. Bio Mater. 2019, 2, 3926−3933.

(27) Nguyen, T. −T. −T.; Belbekhouche, S.; Dubot, P.; Carbonnier, B.; Grande, D. From the Functionalization of Polyelectrolytes to the Development of a Versatile Approach to the Synthesis of Polyelectrolyte Multilayer Films with Enhanced Stability. J. Mater. Chem. A 2017, 5, 24472−24483.

(28) Lundberg, H.; Tinnis, F.; Selander, N.; Adolfsson, H. Catalytic Amide Formation from Non−Activated Carboxylic Acids and Amines. Chem. Soc. Rev. 2014, 43, 2714−2742.

(29) Conversion of a Carboxylic Acid to an Amide; https://chem.libretexts.org/@go/page/5533.

(30) Lanigan, R. M.; Starkov, P.; Sheppard, T. D. Direct Synthesis of Amides from Carboxylic Acids and Amines Using B(OCH2CF3)3. J. Org. Chem. 2013, 78, 4512−4523.

(31) Kim, S.; Huang, J.; Lee, Y.; Hwang, D. S. Complexation and Coacervation of Like−Charged Polyelectrolytes Inspired by Mussels. Proc. Natl. Acad. Sci. U.S.A. 2016, 113, E847−E853.

(32) Wang, Y.; Liu, T.; Yu, T.; Tan, Z.−J.; Zhang, W. Salt Effect on

Thermodynamics and Kinetics of a Single RNA Base Pair. RNA 2020, 26, 470−480.

(33) Wang, Z.; Chen, J.; Wang, L.; Gao, G.; Zhou, Y.; Wang, R.; Xu, T.; Yin, J.; Fu, J. Flexible and Wearable Strain Sensors Based on Tough and Self−Adhesive Ion Conducting Hydrogels. J. Mater. Chem. B 2019, 7, 24−29.

(34) Heidarian, P.; Kouzani, A. Z.; Kaynak, A.; Paulino, M.; Nasri−Nasrabadi, B.; Varley, R. Double Dynamic Cellulose Nanocomposite Hydrogels with Environmentally Adaptive Self−Healing and pH−Tuning Properties. Cellulose 2020, 27, 1407−1422.

(35) Jia, Z.; Lv, X.; Hou, Y.; Wang, K.; Ren, F.; Xu, D.; Wang, Q.; Fan, K.; Xie, C.; Lu, X. Mussel−Inspired Nanozyme Catalyzed Conductive and Self−Setting Hydrogel for Adhesive and Antibacterial Bioelectronics. Bioact. Mater. 2021, 6, 2676−2687.

(36) Gan, D.; Xing, W.; Jiang, L.; Fang, J.; Zhao, C.; Ren, F.; Fang, L.; Wang, K.; Lu, X. Plant−Inspired Adhesive and Tough Hydrogel Based on Ag−Lignin Nanoparticles−Triggered Dynamic Redox Catechol Chemistry. Nat. Commun. 2019, 10, 1487.

(37) Han, L.; Lu, X.; Liu, K.; Wang, K.; Fang, L.; Weng, L.−T.; Zhang, H.; Tang, Y.; Ren, F.; Zhao, C.; Sun, G.; Liang, R.; Li, Z. MusselInspired Adhesive and Tough Hydrogel Based on Nanoclay Confined Dopamine Polymerization. ACS Nano 2017, 11, 2561−2574.

(38) Zhang, D.; Xu, Z.; Li, H.; Fan, C.; Cui, C.; Wu, T.; Xiao, M.; Yang, Y.; Yang, J.; Liu, W. Fabrication of Strong Hydrogel−Bonding Induced Coacervate Adhesive Hydrogels with Antibacterial and Hemostatic Activities. Biomater. Sci. 2020, 8, 1455−1463.

(39) Peng, Q.;Chen, J.; Zeng, Z.; Wang, T.; Xiang, L.; Peng, X.; Liu,

J.; Zeng, H. Adhesive Coacervates Driven by Hydrogen−Bonding Interaction. Small 2020, 16, 2004132.

(40) Han, L.; Wang, M.; Prieto−López, L. O.; Deng, X.; Cui, J. Self−Hydrophobization in a Dynamic Hydrogel for Creating Nonspecific Repeatable Underwater Adhesion. Adv. Funct. Mater. 2020, 30, 1907064.

(41) Ma, C.; Pang, H.; Liu, H.; Yan, Q.; Li, J.; Zhang, S. A Tough, Adhesive, Self−Healable, and Antibacterial Plant−Inspired Hydrogel Based on Pyrogallol−Borax Dynamic Cross−Linking. J. Mater. Chem. B 2021, 9, 4230−4240.

(42) Zhang, Q.; Shi, C.−Y.; Qu, D.−H.; Long, Y.−T.; Feringa, B. L.; Tian, H. Exploring a Naturally Tailored Small Molecule for Stretchable, Self−Healing, and Adhesive Supramolecular Polymers. Sci. Adv. 2018, 4, 8192.

(43) Cui, C.; Chen, X.; Ma, L.; Zhong, Q.; Li, Z.; Mariappan, A.; Zhang, Q.; Cheng, Y.; He, G.; Chen, X.; Dong, Z.; An, L.; Zhang, Y. Polythiourethane Covalent Adaptable Networks for Strong and Reworkable Adhesives and Fully Recyclable Carbon Fiber−Reinforced Composites. ACS Appl. Mater. Interfaces 2020, 12, 47975−47983.

(44) Dalabehera, N. R.; Meher, S.; Palai, B. B.; Sharma, N. K. Instability of Amide Bond with Trifluoroacetic Acid (20%): Synthesis, Conformational Analysis, and Mechanistic Insights into Cleavable Amide Bond Comprising β−Troponylhydrazino Acid. ACS Omega 2020, 5, 26141−26152.

(45) Zhao, M.−H.; Chen, X.−P.; Wang, Q. Wetting Failure of Hydrophilic Surfaces Promoted by Surface Roughness. Sci. Rep. 2014, 4, 5376.

(46) Louzi, V. C.; Campos, J. S. D. C. Corona Treatment Applied to Synthetic Polymeric Monofilaments (PP, PET, and PA-6). Surf. Interfaces 2019, 14, 98-107.

(47) Ding, L.; Wang, L.; Shao, L.; Cao, J.; Bai, Y. The Water-Dependent Decay Mechanism of Biaxially-Oriented Corona-Treated Polyethylene Terephthalate Films. RSC Adv. 2014, 4, 54805-54809.

Chapter 3. Reversible crosslinking of polymer/metal complexes for microfluidics

3.1. Introduction

Chitosan is a polysaccharide obtained from the deacetylation of chitin.[1–3] Based on its unique characteristics, such as hydrophilicity, biocompatibility, and pH responsivity, a wide range of applications, such as drug delivery and sensors, have been developed.[4–9] Especially, this polymer is also capable of capturing heavy metal ions through a coordination bond, so toxic metal ions in aqueous solutions can be easily removed by a chitosan/metal–ion complex.[10, 11] Furthermore, a recyclable water purification system could be achieved using a reversible crosslinking of the chitosan hydrogel. This indicates that chitosan is certainly attractive because this natural polymer could reduce the environmental concern as well.

In relation to chitosan, recyclability could be achieved by a reversible phase transition of physically crosslinked polymers. For example, chitosan becomes dissolved when it is exposed to an acid.[12–16] This is mainly due to water solubility changes determined by the pH level. In detail, chitosan polymers become soluble, accompanying the protonation of NH_2 below pH 6.3 and start to form a gel due to the deprotonation of NH_3^+ above pH 6.3.[13–17] Similarly, coordination bonds between chitosan and transition–metal ions are also related to the pH levels of the solutions. For example, the chitosan/Cu^{2+} hydrogel was obtained above pH 6.3, while the chitosan polymer was soluble in aqueous solutions at the pH level below 6.3 (**Figure 3.1**).[18] This is explained by lone–pair electrons which are donated from NH_2 to transition–metal ions to facilitate their temporary sharing. Therefore, a fundamental task is to determine the behavior of the polymer at different pH levels.

With regard to the gelation of the chitosan hydrogel, previous research studies were focused on the gelation rate using a one–

dimensional gel growth system in an alkali solution.[3, 9-21] Nie et al. reported that a high concentration of NaOH in an alkali led to an elevated growth rate of the chitosan/Cu^{2+} hydrogel. Interestingly, the rapid growth led to an oriented fibrous structure, while a discrete multi-layer was obtained at a low growth rate.[19] Comparably, Dobashi et al. discussed the gelation speed of chitosan polymers in alkalis with theoretical phase-transition dynamics approaches.[20] However, more in-depth studies are still required to clarify the factors as well as the mechanism of chitosan gelation. Fortunately, the color shift of the chitosan/metal-ion complexes is supposed to be a great hint to explain the gelation process.

On the other hand, a few research groups reported chitosan derivatives obtained by chemical modifications for the sake of enhancing the solubility of the chitosan powder.[22-25] For example, Kim et al. suggested that a catechol conjugation process could enhance the solubility of modified chitosan powder in an aqueous solution at pH values up to 7.0.[22] However, previous works did not discuss the case from a hydrogel to a solution as the concept of a reversible phase transition. Besides, the effect of metal-ion binding to the chitosan polymer on the dissolution has been barely studied compared to the gelation. We believe that a comprehensive understanding of the dissolution behavior will contribute to not only establishing the recycle process but also expanding the application field of the chitosan polymer.

Here, we have conducted dynamic studies of the dissolution as well as the gelation of physically crosslinked chitosan/metal-ion complexes. Among metal ions, Cu^{2+} was first considered due to the strong affinity of NH_2 to Cu^{2+}.[26, 27] It is noteworthy that the hydrogels obtained from the gelation test were directly applied to the dissolution test in order to assume the recycling process. Furthermore, a one-dimensional gel growth system and an acetate buffer solution were prepared for the precise analysis of the dominant factors to determine the rates of a phase transition. Lastly, a brief ligand chemistry was utilized in order to understand the

interaction between the polymer and metal ions when a phase transition occurred. The effect of other metal ions (Mn^{2+}, Fe^{3+}, and Ca^{2+}) was also investigated compared to Cu^{2+}. At the end of the study, a microfluidic switch was operated based on the reversible crosslinking of the chitosan/Cu^{2+} hydrogel.

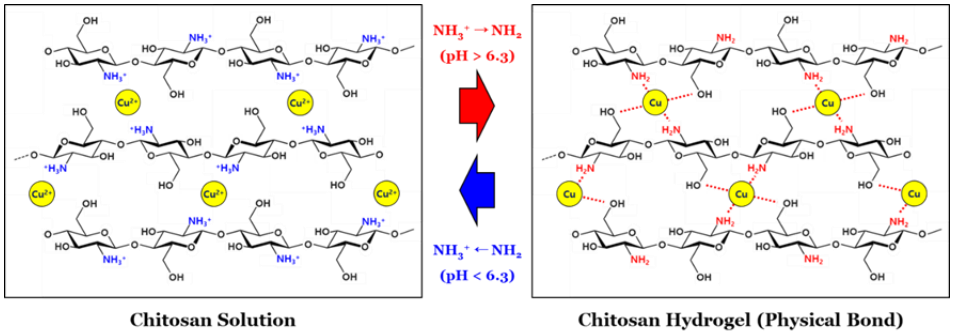

Figure 3.1. Illustration of the reversible crosslinking of the physically crosslinked chitosan/Cu^{2+} hydrogel.

3.2. Experimental section

3.2.1. Materials

Chitosan (Sigma, 448877) was used as a raw hydrogel material. The average viscosity of chitosan is 500 cp (1 wt % in 1 vol % CH_3COOH aqueous solution), and the degree of deacetylation is 75–85 %. Acetic acid (CH_3COOH), sodium acetate (CH_3COONa), sodium hydroxide (NaOH), copper chloride ($CuCl_2$), manganese chloride ($MnCl_2$), iron chloride ($FeCl_3$), calcium chloride ($CaCl_2$), and sodium nitrite ($NaNO_2$) were purchased from Daejung Chemical and Metals Co., Ltd. and were of analytical reagent grade.

3.2.2. Gelation test

Chitosan solution was prepared by dissolving chitosan powder in 2 vol % of a CH_3COOH aqueous solution, with the final concentration of chitosan fixed at 2 wt %. Then, various amounts of $CuCl_2$ powder were added in order to form a chitosan/Cu^{2+} solution with different molar ratios between Cu^{2+} and NH_2 (Cu^{2+}/NH_2 = 0.0–0.5). Each solution was added to a glass mold before being immersed in a clotting bath. Clotting baths were prepared by dissolving various amounts of NaOH pellets in deionized water, with the final concentrations held in the range of 2–20 wt %. The growth of the chitosan/Cu^{2+} hydrogel was started when the chitosan/Cu^{2+} solution was immersed into the NaOH clotting bath. Each of the glass molds (2.5 mL of chitosan/Cu^{2+} solution) should be immersed in at least 500 mL of the NaOH aqueous solution in order to ensure uniform gelation. The chitosan/Cu^{2+} hydrogel growth rate was calculated according to the gel thickness, which was measured every hour. The color change from light blue (chitosan/Cu^{2+} solution) to deep blue (chitosan/Cu^{2+} hydrogel) was observed when the gelation proceeded.

3.2.3. Viscosity measurements

The NaOH aqueous solution (2–10 wt %) as well as the chitosan/Cu^{2+} solution (Cu^{2+}/NH_2 = 0.0, 0.2) were prepared using the method described in section 3.2.2. 40 mL of the chitosan/Cu^{2+} solution was added to a glass mold, and a spindle which

was connected to a rotary viscometer (LVDV−II+, Brookfield) was dipped into the solution. The viscosity of the complex was recorded by adding an aqueous solution of NaOH with a speed of 0.3 mL/min.

3.2.4. Dissolution test

Chitosan/Cu^{2+} hydrogels were prepared using the method described in section 3.2.2. except that the final concentration of NaOH was fixed at 10 wt %. After gelation, chitosan/Cu^{2+} hydrogels were rinsed with deionized water repeatedly and stabilized in a deionized water bath for 24 h before the dissolution test. 1.0 M acetate buffer solutions with pH levels ranging from 3.8 to 5.6 were prepared in order to clarify the effect of the pH on the dissolution speed of the chitosan/Cu^{2+} hydrogel. The relative concentrations of CH_3COOH and CH_3COONa at each pH level were calculated with the Henderson-Hasselbalch equation ($pH = pK_a + log\frac{[A]^-}{[HA]}$, p$K_a$ for acetic acid = 4.75). The prepared buffer solutions were checked with a pH meter (Star A2116, Thermo Scientific). Then, various amounts of $NaNO_2$ powder were added with different molar ratios between NO_2^- and Cu^{2+} (NO_2^-/Cu^{2+} = 0−90). The prepared chitosan/Cu^{2+} hydrogels were immersed in buffer solutions with a stirring speed of 300 rpm at room temperature. Every 1.0 g of the chitosan/Cu^{2+} hydrogel should be immersed in 10 mL of the buffer solution under each condition. In order to confirm the complete disintegration quantitatively, the viscosity of the environmental buffer solution was measured using a rotary viscometer. The viscosity gradually increased as the chitosan hydrogel disintegrated into the buffer solution. Finally, the complete dissolution was determined when the viscosity became constant without any residual chitosan/Cu^{2+} hydrogel. Here, t_{90}, the time to reach 90 % of the converging value after Weibull fitting, was considered as the dissolution time.

3.2.5. Fluidic switching test

A cross−shaped fluidic test tube was assembled with transparent polypropylene tubes and a four−way connector. Both tubes and the connector are capable of operating in aqueous solutions ranging from the acidic to basic pH level. The inner radius of the four−way

connector was 1 mm. Water flowed through a vertical line at a rate of 30 mL/min. Other tubes perpendicular to the water flow line were connected to syringes with chitosan/Cu^{2+} solution and NaOH solution. To close the water line, 0.02 g/mL of the chitosan/Cu^{2+} solution (Cu^{2+}/NH_2 = 0.2) and NaOH (0, 2, 10 wt %) aqueous solutions were simultaneously injected. The injection rate for both syringes was fixed at 20 mL/min. The water flow rate was calculated according to the amount of water which flowed in an operating interval. To reopen the water line, a CH_3COOH (0, 10 vol %)/NO_2^- (0.0, 1.5 M) aqueous solution was used. A Y-shaped bypass was connected to make a static flow of CH_3COOH/NO_2^- solution near the blocking gel. 20 mL/min was used as an injection speed of CH_3COOH/NO_2^- solution.

3.2.6. Microfluidic switching test

A seven-hole microfluidic channel was fabricated by patterning PDMS (Sylgard 184, Dow Corning) on glass. The patterned PDMS was developed by a facile photolithography technique in order to control the channel structure. The final dimensions of the microfluidic channel were fixed at 300 μm × 50 μm (width × depth). Permanent bonding between PDMS and the glass was obtained via a plasma bonding step after rinsing these surfaces with an acetone/ethanol solution. Additional heat (60 °C) and pressure (6500 N/m^2) were applied to the PDMS/glass device for 48 h. The microfluidic switching test was operated under similar conditions in section 3.2.5, except for the final concentration of chitosan/Cu^{2+} solution (0.005 g/mL, Cu^{2+}/NH_2 = 0.2) and flow rate (150 μL/min).

3.3. Results and discussion

3.3.1. Gelation of the chitosan/Cu^{2+} hydrogel

As shown in **Figure 3.2a**, the chitosan/Cu^{2+} hydrogel formation rate was analyzed through a one-dimensional gelation system. A glass mold filled with the chitosan/Cu^{2+} solution and a clotting bath in which NaOH was dissolved were both prepared. The chitosan/Cu^{2+} solution started to form a gel as soon as the glass mold

was immersed in the clotting bath. As described in **Figure 3.2d**, a solution region under a gel layer decreased during gel growth and the completely grown chitosan/Cu^{2+} hydrogel was finally obtained. Then, a one-dimensional grown part was verified using the rheological characterization. The values of the storage modulus were always higher than those of the loss modulus regardless of Cu^{2+}, which indicated that the hydrogel was successfully fabricated (**Figure 3.3**). Besides, the gelation process was visual because Cu^{2+} dissolved in the chitosan polymer solution took part in the gelation through coordination bonding between NH_2 and Cu^{2+} considering the color change from light blue (chitosan/Cu^{2+} solution) to deep blue (chitosan/Cu^{2+} hydrogel). The origin of different colors is that NH_2 caused more splitting of the d-orbital of Cu^{2+} than water (H_2O), as the N atoms in NH_2 were more electropositive than the O atoms in H_2O. As a result, the chitosan/Cu^{2+} hydrogel absorbed higher energy corresponding to yellow light, the complementary color of deep blue.[28,29]

For the chitosan polymers, they are able to become a physically crosslinked gel when NH_3^+ is deprotonated to NH_2 on aqueous surfaces under alkaline conditions. Therefore, the rate of deprotonation from NH_3^+ to NH_2 should be a major factor affecting the chitosan hydrogel formation outcome. As shown in **Figure 3.2b**, the time courses of gel growth indicated that an increase in the concentration of NaOH led to rapid growth of the gel. This can be explained by the higher diffusion rate of OH^- through the grown hydrogel layer in order to deprotonate NH_3^+ at the sol/gel interface. The 2 wt % NaOH aqueous solution required more than 72 h until gelation was fully complete owing to the low diffusion rate of OH^-. Apparently, the chitosan gel growth rate strongly depended on the concentration of NaOH. From a similar point of view, we predicted that a small amount of acetic acid in chitosan solution could also be supportive in order to promote the gel growth. According to the previous work reported by Dobashi et al., a large amount of acetic

acid in the chitosan solution interrupted the chitosan gel growth due to a delay in the deprotonation of NH_3^+ at the sol/gel interface.[20]

On the other hand, the influence of the concentration of Cu^{2+} (Cu^{2+}/NH_2 = 0.0−0.5) on the gel formation rate with the same concentration of NaOH was mostly negligible (**Figure 3.2c, d**). This result was quite reasonable in that coordination bonding can form only when lone−pair electrons are shared between NH_2 and Cu^{2+}. **Figure 3.4** clearly indicates that a chitosan/Cu^{2+} hydrogel with a large amount of Cu^{2+} (Cu^{2+}/NH_2 = 1.0) also grew at a speed identical to that of a pure chitosan hydrogel in the 20 wt % NaOH aqueous solution. Moreover, we investigated the gelation behavior with different metal ions (Cu^{2+}, Mn^{2+}, Fe^{3+}, and Ca^{2+}) incorporated with the chitosan polymer (**Figure 3.5**). In brief, the chitosan/metal−ion gel (metal ion/NH_2 = 0.2) growth rate was undoubtedly accelerated when the concentration of NaOH became high. For example, the chitosan/Fe^{3+} hydrogel grew faster in 10 wt % NaOH aqueous solution compared to 5 wt % NaOH aqueous solution. However, each chitosan/metal−ion hydrogel grew at a different rate, which followed the order of $Fe^{3+} \approx Cu^{2+} > Mn^{2+} \approx Ca^{2+}$. This was probably caused by the change of affinity of NH_2 to metal ions. According the previous report, ethylenediamine favored Fe^{3+} and Cu^{2+} rather than Mn^{2+} and Ca^{2+}.[27] This probably resulted in byproducts such as $Mn(OH)_2$ and $Ca(OH)_2$, which interrupted the diffusion of OH^-. As explained by Nie et al., $Ca(OH)_2$ precipitation within the chitosan hydrogel was clearly observed.[19] The result indicated that the strong affinity of NH_2 to Cu^{2+} encouraged the growth of the chitosan/Cu^{2+} hydrogel.

Next, the viscosity changes of the chitosan/Cu^{2+} complexes (Cu^{2+}/NH_2 = 0.0, 0.2) with sequential drops of aqueous NaOH solutions (0−10 wt %) were measured (**Figure 3.6**). As shown in **Figure 3.6a**, a rotary viscometer was utilized and the viscosity was recorded until the spindle became unrotated (**Figure 3.6d, e**). Even though the viscosity measurement was inadequate in spatially heterogeneous complexes, it could express a torque in the hydrogel, hindering the rotation of the spindle. In detail, a piece of hydrogel

nucleated at the surface of the solution started to merge with each other and interrupt the rotation of the spindle so that the rapid gel formation led to a sharp increase in torque which was expressed by the viscosity. Therefore, the viscosity fluctuations of the chitosan/Cu^{2+} complex may indicate how rapidly the gel growth proceeded. However, we used representative viscosity measured in the whole sample because it was impossible to detect the values of the heterogeneous regions during gelation. **Figure 3.6b, c** clearly shows that the slope corresponding to the 10 wt % NaOH aqueous solution was much steeper than the others (2 and 5 wt %). This result indicates that gel characteristics were more quickly obtained when a higher concentration of NaOH aqueous solution was added. This can also be explained by the higher diffusion rate of OH^-, resulting in rapid gel formation. It was quite analogous to the gelation test in **Figure 3.2** in that the concentration of the NaOH aqueous solution determined the speed of the gelation. However, the time scale was shorter compared to **Figure 3.2**, because the viscosity of the complexes exceeded a maximum range of the measurement promptly during the gelation processes. Apart from the gel formation rate, it was also found that the chitosan/Cu^{2+} complex (**Figure 3.6c**) tended to show higher viscosity than the pure chitosan hydrogel (**Figure 3.6b**) when the same amount of NaOH aqueous solution was dropped. This was mainly due to the stronger crosslinking of chitosan polymers with the help of Cu^{2+}, which greatly hinders the rotation of the spindle. The much higher storage modulus of the chitosan/Cu^{2+} hydrogel (Cu^{2+}/NH_2 = 0.2) than the pure chitosan hydrogel (Cu^{2+}/NH_2 = 0.0) could be other evidence of the strong crosslinking through coordination bonding (**Figure 3.3**).

In conclusion, the higher diffusion rate of OH^- was the dominant driving force of the physical gelation of chitosan/Cu^{2+} regardless of the concentration of Cu^{2+}. However, the Cu^{2+} within the chitosan polymers accelerated the gaining of gel characteristics.

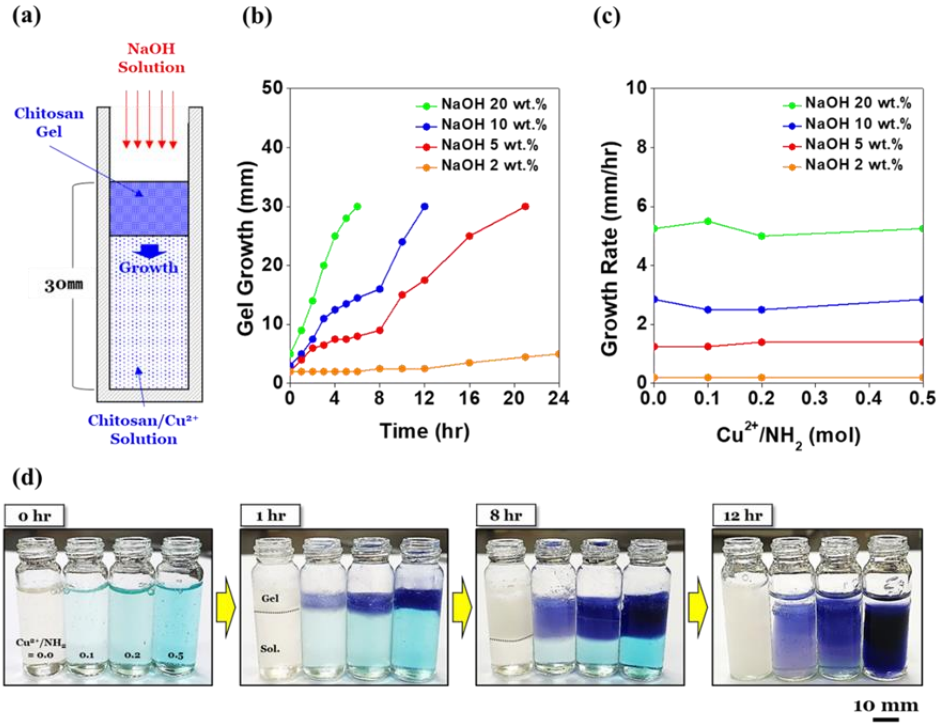

Figure 3.2. Gelation test of the chitosan/Cu^{2+} hydrogel: (a) Schematic description of a one-dimensional chitosan/Cu^{2+} hydrogel grown in contact with the NaOH aqueous solution. (b) Time courses of the chitosan/Cu^{2+} hydrogel (Cu^{2+}/NH_2 = 0.2) with concentrations of 2 ~ 20 wt.% NaOH over a time of 24 hr. (c) Growth rate of chitosan/Cu^{2+} hydrogels (Cu^{2+}/NH_2 = 0.0 ~ 0.5) with concentrations of 2 ~ 20 wt.% NaOH. (d) Photos of growing chitosan/Cu^{2+} hydrogel samples (Cu^{2+}/NH_2 = 0.0 ~ 0.5) in contact with a 10 wt.% NaOH aqueous solution. NH_2 caused higher energy absorption compared to H_2O such that the color change from light blue (chitosan/Cu^{2+} solution) to deep blue (chitosan/Cu^{2+} hydrogel) occurred.

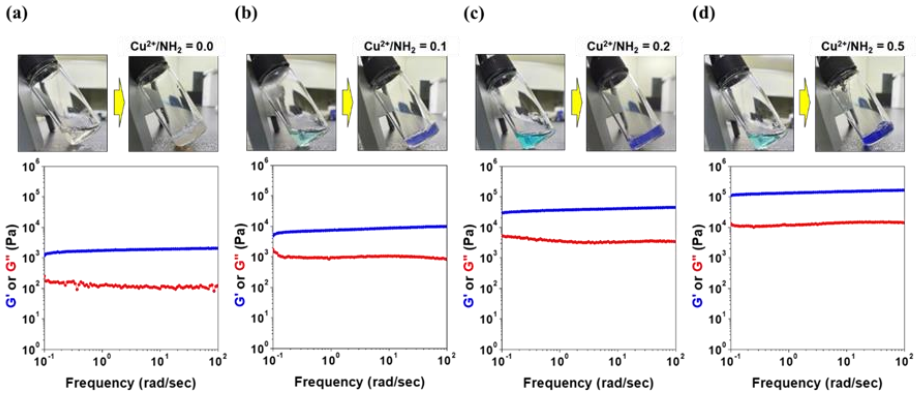

Figure 3.3. Rheological properties of the chitosan/Cu^{2+} hydrogels with Cu^{2+}/NH_2 (a) 0.0 (b) 0.1 (c) 0.2 (d) 0.5.

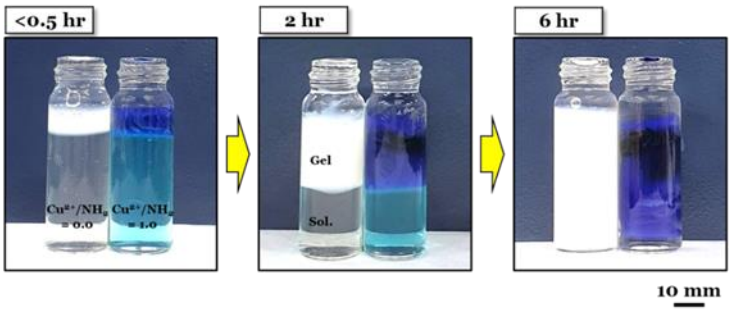

Figure 3.4. Gelation test of the chitosan/Cu^{2+} hydrogel.

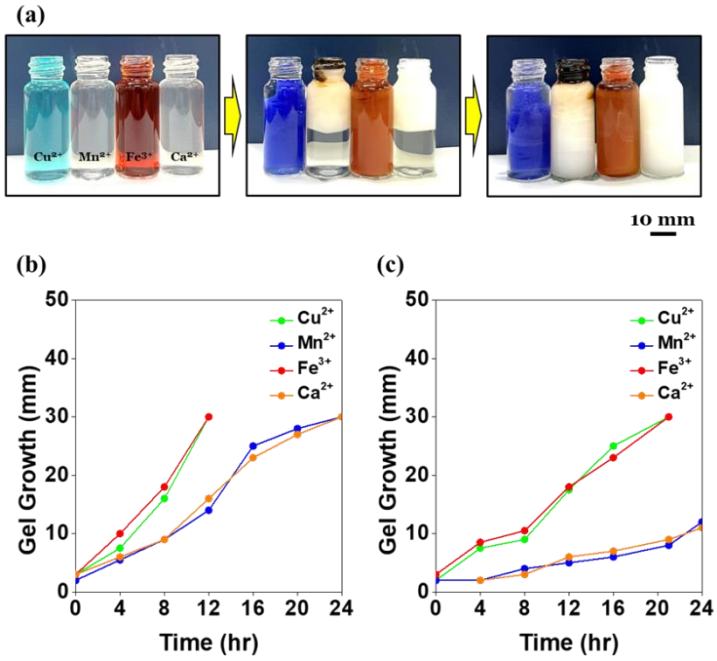

Figure 3.5. Gelation test of the chitosan/metal−ion (Cu^{2+}, Mn^{2+}, Fe^{3+}, and Ca^{2+}) hydrogel: (a) Photos of growing chitosan/metal−ion hydrogel samples (metal−ion/NH_2 = 0.2) in contact with a 10 wt.% NaOH aqueous solution. (b) Time courses of the chitosan/metal−ion hydrogel (metal−ion/NH_2 = 0.2) with concentrations of 10 wt.% NaOH over a time of 24 hr. (c) Time courses of the chitosan/metal−ion hydrogel (metal−ion/NH_2 = 0.2) with concentrations of 5 wt.% NaOH over a time of 24 hr.

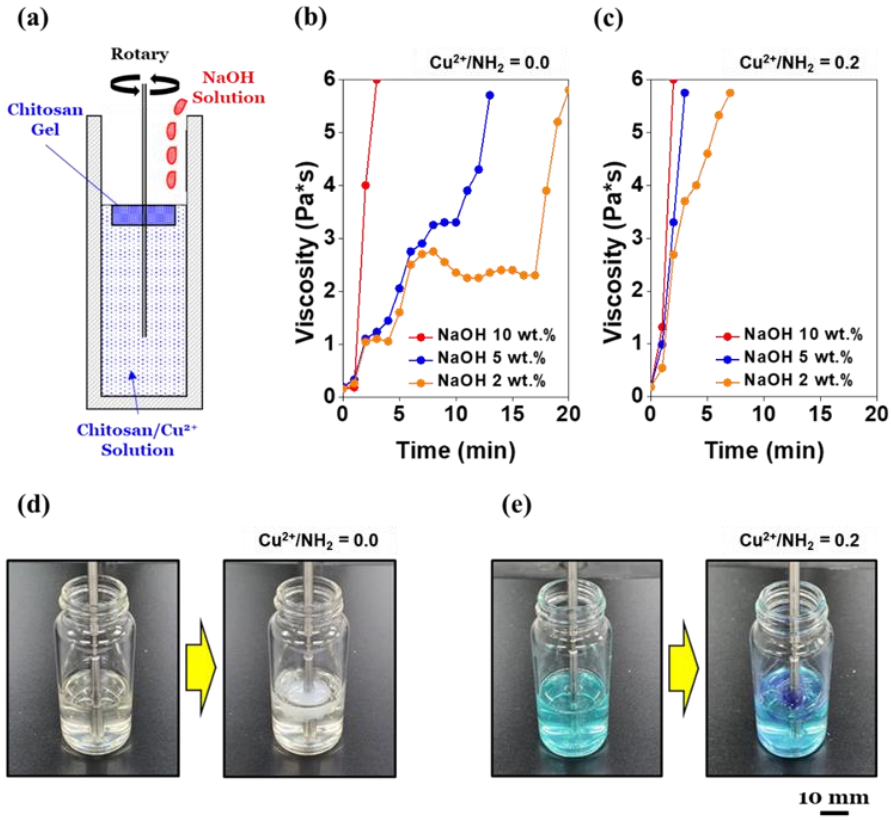

Figure 3.6. Viscosity measurements of the chitosan/Cu^{2+} hydrogel: (a) Schematic description of a rotary viscometer system using the chitosan/Cu^{2+} hydrogel with sequential drops (0.3 ml/min) of a NaOH aqueous solution. (b) Time courses of the pure chitosan hydrogel (Cu^{2+}/NH_2 = 0.0) at concentrations of 0 ~ 10 wt.% NaOH. (c) Time courses of the chitosan/Cu^{2+} hydrogel (Cu^{2+}/NH_2 = 0.2) at concentrations of 0 ~ 10 wt.% NaOH. (d) Photos of the initial and final states of the pure chitosan hydrogel (Cu^{2+}/NH_2 = 0.0). (e) Photos of the initial and final states of the chitosan/Cu^{2+} hydrogel (Cu^{2+}/NH_2 = 0.2).

3.3.2. Dissolution of the chitosan/Cu^{2+} hydrogel

Before the dissolution test, chitosan/Cu^{2+} hydrogels with various compositions (Cu^{2+}/NH_2 = 0.0–0.5) were prepared using the 10 wt % NaOH aqueous solution with the one-dimensional gelation system. That is to say, the hydrogels obtained from the gelation test were applied to the dissolution test as the concept of the recyclable process. Then, factors that disintegrate a physically crosslinked chitosan/Cu^{2+} hydrogel were analyzed using 1.0 M acetate buffer solution system with pH levels from 3.8 to 5.6 accompanied by mechanical stirring (**Figure 3.7a**). This pH range should be suitable for a dissolution test of the chitosan hydrogel considering its pK_a value of 6.3. Even though citrate buffer solution could also provide the useful pH levels from 3.0 to 6.2, the chitosan polymer was not dissolved well, probably due to the strong ionic strength of the solution (**Table 3.1**).[30] Besides, the viscosity was measured using a rotary viscometer in order to analyze the dissolution quantitatively. In detail, 1.0 g of the chitosan hydrogel was immersed in 10 mL of the buffer solution whose initial viscosity was 3.5 ± 0.7 mPa s. After that, the viscosity of the solution in which the chitosan polymer disintegrated gradually increased until the hydrogel was completely dissolved. Then, the viscosity uniformly converged at 9.4 ± 1.0 mPa s because the final concentration of the chitosan polymer was equal. Therefore, the convergence of the viscosity without any residual chitosan/Cu^{2+} hydrogel indicated the complete dissolution. Here, t_{90} was considered as the dissolution time. As shown in **Figure 3.7a**, t_{90} was defined as the time to reach 90 % of the converging value after Weibull fitting. Even though the heterogeneous regions should exist during dissolution, we reported the viscosity measured in the solution representatively.

Figure 3.8 shows the result of the dissolution test described in **Figure 3.7**. Contrary to gelation, the rate of protonation from NH_2 to NH_3^+ should be a major factor affecting the chitosan hydrogel dissolution outcome. As shown in **Figure 3.8a**, a decrease in the pH level powered the dissolution rate significantly. Fortunately, there

was no distinct change in the pH level during the dissolution of the chitosan/Cu^{2+} hydrogel due to the acetate buffer solution.

Next, two additional key factors which regulate the dissolution rate of the chitosan/Cu^{2+} hydrogel were discovered. The chitosan/Cu^{2+} hydrogel dissolved slowly as the concentration of Cu^{2+} increased. Moreover, Cu^{2+} led to a lower maximum pH level, at which point the chitosan/Cu^{2+} hydrogel was completely disintegrated. For example, the chitosan/Cu^{2+} hydrogel (Cu^{2+}/NH_2 = 0.2, 0.5) remained swollen at pH levels ranging from 5.2 to 5.6, where the pure chitosan hydrogel could be perfectly soluble (**Figure 3.8a**). This implies that strong binding within the polymers induced by coordination complexes required an intense driving force in order to disintegrate. Fortunately, the metal–ion affinity of molecules could be utilized for the purpose of enhancing the dissolution rate as a ligand exchange from weaker molecules to stronger molecules generally occurs in an aqueous solution.[31–33] Given the primary requirements such as metal–ion affinity, water solubility, and pK_a, NO_2^- was regarded as an excellent molecule. Theoretically, N atoms in NO_2^-, which have electronegative O atoms, show stronger metal–ion affinity than N atoms in NH_2 such that Cu^{2+} prefers NO_2^- to NH_2.[29,31–34] Despite the fact that there are a few ligand molecules with stronger metal–ion affinity than NH_2, they were not suitable for chitosan/Cu^{2+} hydrogel dissolution (**Table 3.2**). For example, 2,2′–bipyridine is insoluble in water and cyanide ions are weakly acidic with a pK_a of 9.2. Here, $NaNO_2$ was used as the source of NO_2^-, and its high solubility in water was readily confirmed, more than 50 g/100 mL. As expected, NO_2^- dissociated from $NaNO_2$ enhanced the dissolution of the chitosan/Cu^{2+} hydrogel, and it is shown in **Figure 3.8b**. In detail, the dissolution rate increased dramatically as higher concentrations of NO_2^- (NO_2^-/Cu^{2+} = 0–90) were utilized at the same pH level. In addition, the maximum pH level at which a fully disintegrated solution was obtained tended to be elevated when NO_2^- was applied. For example, the chitosan/Cu^{2+} hydrogel (Cu^{2+}/NH_2 = 0.2) could be completely dissolved at pH levels ranging

from 5.0 to 5.6 when NO_2^- was utilized (NO_2^-/Cu^{2+} = 9–90), while it remained swollen at a pH level above 5.0 without NO_2^- (NO_2^-/Cu^{2+} = 0). The strong effect of NO_2^- was investigated when other metal ions (Mn^{2+}, Fe^{3+}, and Ca^{2+}) were utilized instead of Cu^{2+} (**Table 3.3**). For example, it took at most 50 min to dissolve the chitosan/Fe^{3+} hydrogel (Fe^{3+}/NH_2 = 0.2) at pH 5 with NO_2^- (NO_2^-/Mn^{2+} = 90), while the same hydrogel was completely disintegrated after 450 min at pH 5 without NO_2^-. However, it was especially notable that metal ions apparently affected the dissolution rate of the chitosan/metal–ion hydrogels, probably due to the different affinity of NH_2 to metal ions.[26,27] For example, the chitosan/Ca^{2+} hydrogel tended to be dissolved faster than others, and this was probably because of the weak affinity of NH_2 to Ca^{2+} caused by the absence of the d–orbital (not the transition metal).[19]

Interestingly, NO_2^- did not work when the pure chitosan hydrogel was dissolved (Cu^{2+}/NH_2 = 0.0). For example, a converging time at pH 5 was not significantly affected by NO_2^- (NO_2^-/Cu^{2+} = 0, ∞), as shown in **Figure 3.7b**. This was a major difference in that NO_2^- (NO_2^-/Cu^{2+} = 9) shortens the converging time of the viscosity when chitosan/Cu^{2+} (Cu^{2+}/NH_2 = 0.2, 0.5) was dissolved (**Figure 3.7c, d**). **Figure 3.9** shows the significant effect of NO_2^- on the chitosan/Cu^{2+} hydrogel dissolution visually. This can be explained by the interaction between the ligand molecules and the metal ions. In detail, Cu^{2+} could be favorably extracted from strong binding to chitosan polymers with the aid of NO_2^-, which has stronger metal–ion affinity compared to NH_2,[29,31–34] while the pure chitosan polymer was not affected by the ligand molecules. In fact, different colors of the chitosan/Cu^{2+} solution which considerably depended on the ligand molecules could be other evidence of the suggested mechanism. As shown in **Figure 3.7e**, chitosan/Cu^{2+} dissolved in the CH_3COOH/NO_2^- aqueous solution was light green in color,[35–37] while chitosan/Cu^{2+} dissolved in the CH_3COOH aqueous solution was light blue. The reason for the different colors can be explained as in section 3.3.1. In practice, the color of the Cu^{2+}/NO_2^- ($CuCl_2/NaNO_2$)

aqueous solution was greenish, whereas the Cu^{2+}/NH_2 (ethylene-diamine) aqueous solution was bluish. However, the dissolution of the chitosan/Cu^{2+} hydrogel was not expected at a pH level above 6.3, even with NO_2^-, mainly because chitosan polymers could not become hydrated unless protonation occurred.

In conclusion, two other factors can clearly be involved when the chitosan/Cu^{2+} hydrogel was intended to be dissolved at a pH below 5.6. Cu^{2+}, which contributed to stronger crosslinking, led to a slower dissolution, while NO_2^-, which tended to attract Cu^{2+}, accelerated the dissolution process dramatically. Particularly, NO_2^- could help the chitosan/Cu^{2+} hydrogel dissolve faster compared to the pure chitosan hydrogel.

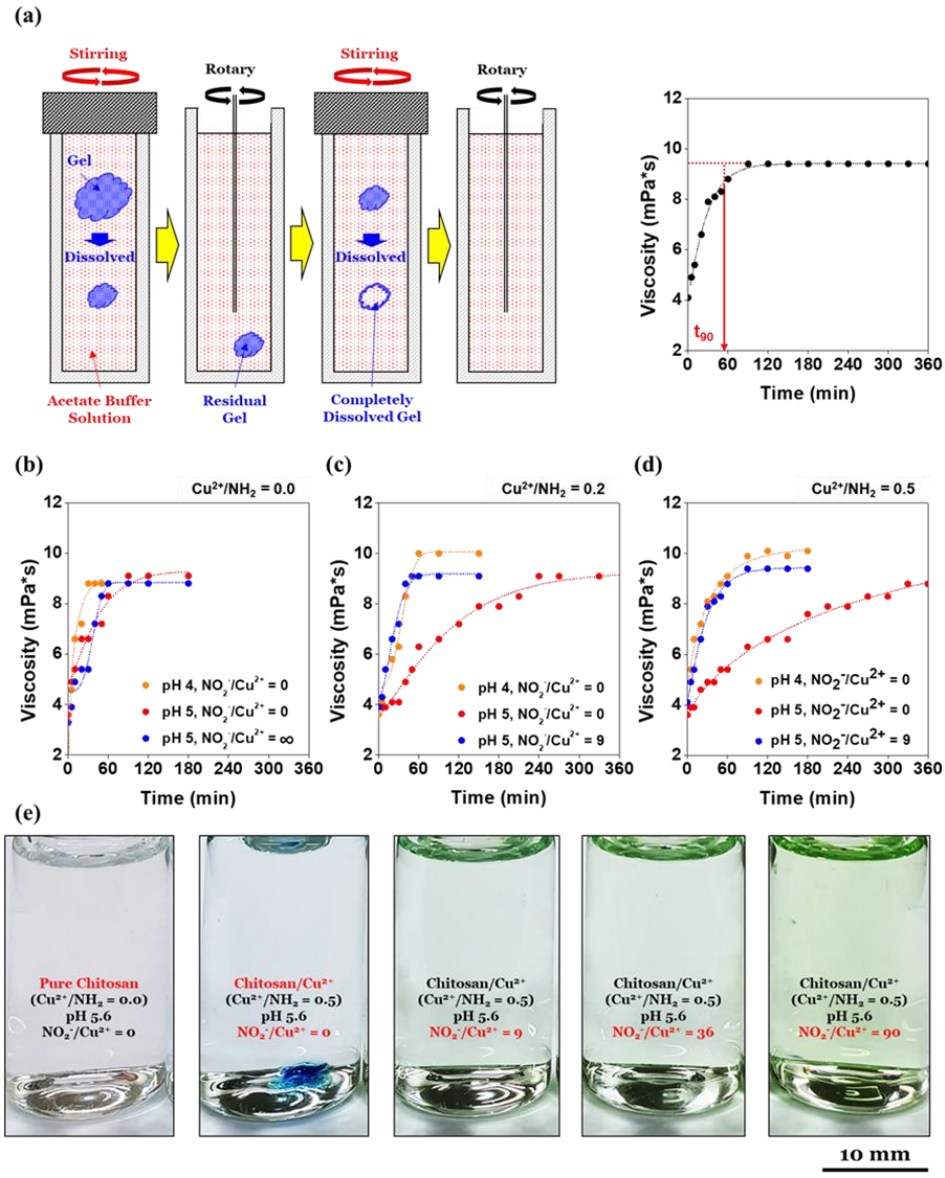

Figure 3.7. Viscosity measurements of the chitosan/Cu^{2+} hydrogel dissolution and solution color comparison: (a) Schematic description of chitosan/Cu^{2+} hydrogel dissolution using an acetate buffer solution system with pH levels ranging from 3.8 to 5.6 and viscosity measurements. Here, t_{90}, the time to reach 90 % of the converging value after Weibull fitting, was considered as the dissolution time. (b) Time courses of pure chitosan hydrogel (Cu^{2+}/NH_2 = 0.0) dissolution in acetate buffer solutions (pH 4, 5 and NO_2^-/Cu = 0, ∞). (c) Time

courses of chitosan/Cu^{2+} hydrogel (Cu^{2+}/NH_2 = 0.2) dissolution in acetate buffer solutions (pH 4, 5 and NO_2^-/Cu = 0, 9). (d) Time courses of chitosan/Cu^{2+} hydrogel (Cu^{2+}/NH_2 = 0.5) dissolution in acetate buffer solutions (pH 4, 5 and NO_2^-/Cu = 0, 9). (e) Photos of solutions with different colors after chitosan/Cu^{2+} hydrogel (Cu^{2+}/NH_2 = 0.0, 0.5) dissolution in acetate buffer solutions (pH 5.6, NO_2^-/Cu^{2+} = 0 ~ 90). NO_2^- caused higher energy absorption compared to NH_2 such that Cu/NO_2^- aqueous solution was not bluish, but greenish. The residual chitosan/Cu^{2+} hydrogel (Cu^{2+}/NH_2 = 0.5) was observed when NO_2^- was not utilized at pH 5.6 (NO_2^-/Cu^{2+} = 0).

Dissolution Time (min)	**1.0 M Acetate** (pH 3.8~5.6)			**1.0 M Citrate** (pH 3.0~6.2)				
	pH 4.0	**pH 5.0**	**pH 5.6**	**pH 3.0**	**pH 4.0**	**pH 5.0**	**pH 5.6**	**pH 6.0**
Pure Chitosan (Cu^{2+}/NH_2 = 0.0)	15	60	180	10	N/A	N/A	N/A	N/A
Chitosan/Cu^{2+}(Cu^{2+}/NH_2 = 0.2)	60	240	N/A	30	N/A	N/A	N/A	N/A

Table 3.1. Comparison of aqueous buffer solutions.

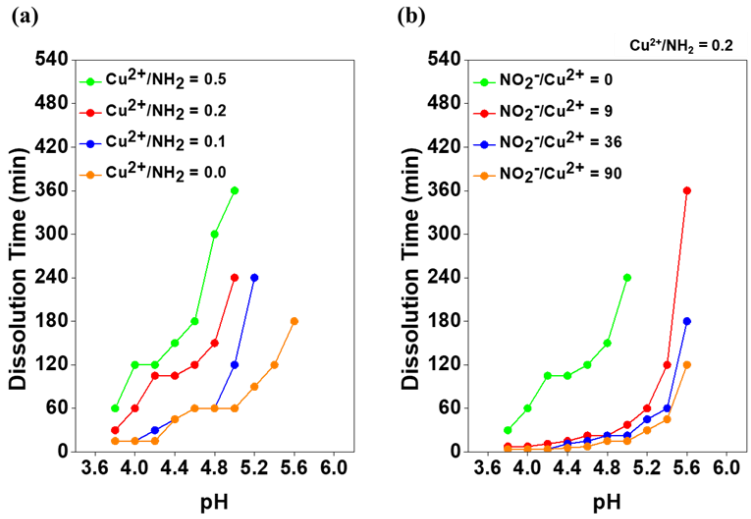

Figure 3.8. Dissolution test of chitosan/Cu^{2+} hydrogel: (a) Influence of Cu^{2+} within chitosan polymers on the chitosan/Cu^{2+} hydrogel (Cu^{2+}/NH_2 = 0.0 ~ 0.5) dissolution process. In this experiment, NO_2^- was not included in the acetate buffer solution. (b) Influence of NO_2^- which was dissolved in an acetate buffer solution (NO_2^-/Cu^{2+} = 0 ~ 90) on the chitosan/Cu^{2+} hydrogel (Cu^{2+}/NH_2 = 0.2) dissolution process.

	Chitosan	**Ligand Molecule** (by metal-ion affinity, strong affinity right)			
	Amine	**Ethylenediamine**	**2,2′-Bipyridine**	**Nitrite**	**Cyanide**
Formula	$\mathbf{N}H_2$	$\mathbf{N}H_2$-CH_2-CH_2-$\mathbf{N}H_2$	$\mathbf{N}C_5H_4$-$C_5H_4\mathbf{N}$	$\mathbf{N}O_2^-$	$\mathbf{C}\equiv N^-$
Water Solubility (25℃, g/ml)	-	1.00	<0.01	0.84 ($NaNO_2$)	>50 (NaCN)
pKa	6.3	10.7 (1st)	4.3 (1st)	3.3	9.2

Table 3.2. Comparison of ligand molecules.

Dissolution time (min)	**Chitosan/Cu^{2+}** (Cu^{2+}/NH_2 = 0.2)	**Chitosan/Mn^{2+}** (Mn^{2+}/NH_2 = 0.2)	**Chitosan/Fe^{3+}** (Fe^{3+}/NH_2 = 0.2)	**Chitosan/Ca^{2+}** (Ca^{2+}/NH_2 = 0.2)
pH 5 (without NO_2^-)	240	300	450	90
pH 5+NO_2^- (NO_2^-/metal-ion = 90)	15	25	50	<5

Table 3.3. Dissolution test of the chitosan/metal−ion (Cu^{2+}, Mn^{2+}, Fe^{3+}, and Ca^{2+}) hydrogel.

Figure 3.9. Dissolution test of the chitosan/Cu^{2+} hydrogel.

3.3.3. Reversible crosslinking for a fluidic switch

A fluidic switch for water flow regulation was operated by means of the reversible crosslinking of the chitosan/Cu^{2+} hydrogel. **Figure 3.10** shows the simple construction of the fluidic switch system which was operated via the reversible crosslinking of chitosan/Cu^{2+} complexes.

A water flow at a rate of 30 mL/min was blocked only when gelation occurred at the connector intersection. Then, all the water (30 mL/min) started to flow along the detour route in 5 s (**Figure 3.11a**, blue symbol). In order to form the gel, the 0.02 g/mL chitosan/Cu^{2+} solution (Cu^{2+}/NH_2 = 0.2) and a 10 wt % NaOH aqueous solution were injected simultaneously at a rate of 20 mL/min from opposite directions perpendicular to the water flow line. A blue gel then successfully formed despite the continual supply of water (**Figure 3.11a**). However, the fluidic switch did not work when an insufficient amount of OH^- was injected due to the slow gel formation rate. For example, the 2 wt % NaOH aqueous solution did not result in rapid gel formation such that water continued to flow with a slight hindering of the flow rate (**Figure 3.11a**, red symbol).

After the water flow was blocked by successful gel formation, an open test was implemented. The water flow rate increased instantly to 30 mL/min as soon as the gel was removed when the CH_3COOH/NO_2^- aqueous solution was steadily injected instead of the chitosan/Cu^{2+} solution and the NaOH aqueous solution. In addition, partially dissolved chitosan polymers were readily found at the outlet. Interestingly, a high concentration of CH_3COOH and NO_2^- tended to shorten the operating time until the channel opened completely, while pure water at a rate of 30 mL/min from the water supply was not capable of removing the chitosan/Cu^{2+} hydrogel, which blocked the water flow (**Figure 3.11b**). This indicates that the chitosan/Cu^{2+} hydrogel not only was strong enough to endure the solvent pressure but was also reversible for a fluidic switch application. However, a small area of the aqueous surface in acidic conditions and the absence of mechanical stirring led to a slow switchover from closed to open.

For example, it took more than 70 s until the channel was fully opened even when 1.5 M of NO_2^- was utilized (**Figure 3.11b**, blue symbol). Note that Y-shaped connectors were used when injecting the CH_3COOH/NO_2^- aqueous solution in order to verify the effect of the dissolution rate clearly without pressure on the blocking gel.

As a result, the fluidic switch was demonstrated based on the reversible phase transition of the chitosan/Cu^{2+} hydrogel. Furthermore, factors that regulated the rates of gelation or dissolution were found to be useful when operating the fluidic switch.

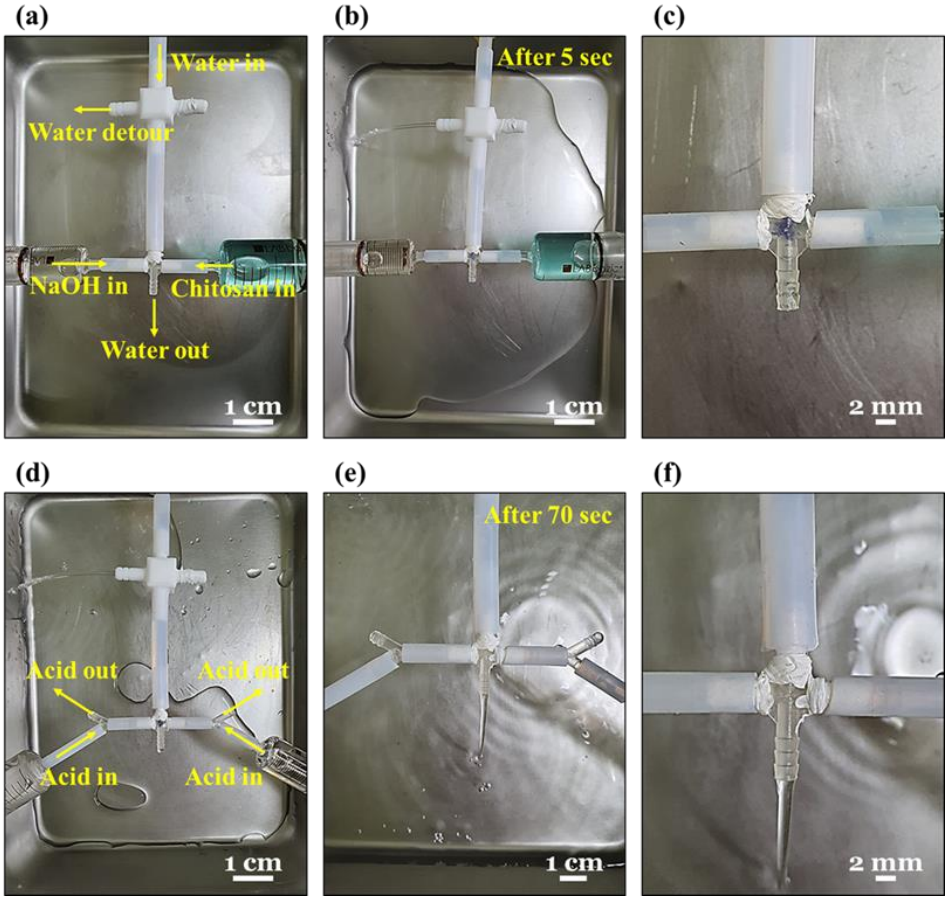

Figure 3.10. Fluidic switch test using reversible crosslinking: (a) Preparation of the fluidic switch test (b) Close under alkali (c) The blue gel when close (d) Acidic solvents for open (e) Open (f) The blue gel removed when open.

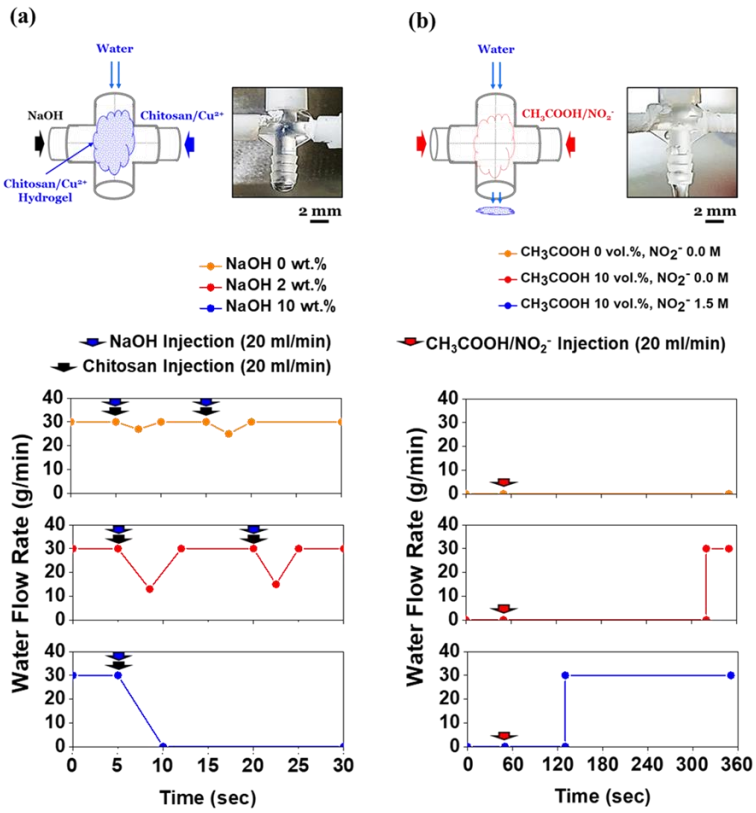

Figure 3.11. Fluidic switch test with the reversible crosslinking of the chitosan/Cu^{2+} hydrogel: the water flow rate was fixed at 30 ml/min. (a) Close test (gelation) with concentrations of 0 ~ 10 wt.% NaOH. The chitosan/Cu^{2+} solution and a NaOH aqueous solution were injected simultaneously to form a gel. (b) Open test (dissolution) with a CH_3COOH (0, 10 wt.%)/NO_2^- (0, 1.5 M) aqueous solution after the channel in (a) was blocked.

3.3.4. Microfluidic switch

For a space-saving device to be used in narrow and sophisticated channels, the solution-based fluidic switch system is expected to be advantageous compared to a mechanical valve or a tiny gear.[38-43] As a demonstration, a seven-hole microfluidic channel was fabricated using patterned PDMS on a glass substrate (**Figure 3.12a, e**). The channel structure was designed using a facile photolithography technique, and the attachment of PDMS/glass was achieved after a plasma treatment (**Figure 3.13**).[44-47] The final dimensions of the channel were set to 300 μm × 50 μm (width × depth), and an initial water flow check was implemented before the switch test (**Figure 3.12b**).

When the 0.005 g/mL chitosan/Cu^{2+} solution and the 10 wt % NaOH aqueous solution were injected from both sides, all the water (150 μL/min) started to flow along the detour route in 5 s (**Figure 3.12c**). **Figure 3.12f** shows the chitosan/Cu^{2+} hydrogel part which directly formed near the intersection immediately after the injection of the two solutions. In particular, the gel was not removed until the acidic aqueous solution was injected instead of the NaOH aqueous solution. For example, the CH_3COOH/NO_2^- aqueous solution with a final concentration of 10 wt %/1.5 M led to a smooth water flow without any congestion in 15 s (**Figure 3.12d**). One aspect that differed from the fluidic switch described in section 3.3.3 was the quick switchover from closed to open. We considered that this arose due to the low concentration of the chitosan/Cu^{2+} solution. In fact, a chitosan solution with high viscosity could not be injected through the microfluidic channel. Therefore, we held its concentration in the range from 0.02 to 0.005 g/mL. From a simple estimation, there was approximately 25% of NH_2 to be protonated compared to the case described in section 3.3.3.

As a result, this demonstration indicates that the reversible crosslinking of the chitosan/Cu^{2+} hydrogel can be applied to a microfluidic switch to regulate a water flow readily. Furthermore,

reproducibility as well as quick switchover can be achieved in a microfluidic channel.

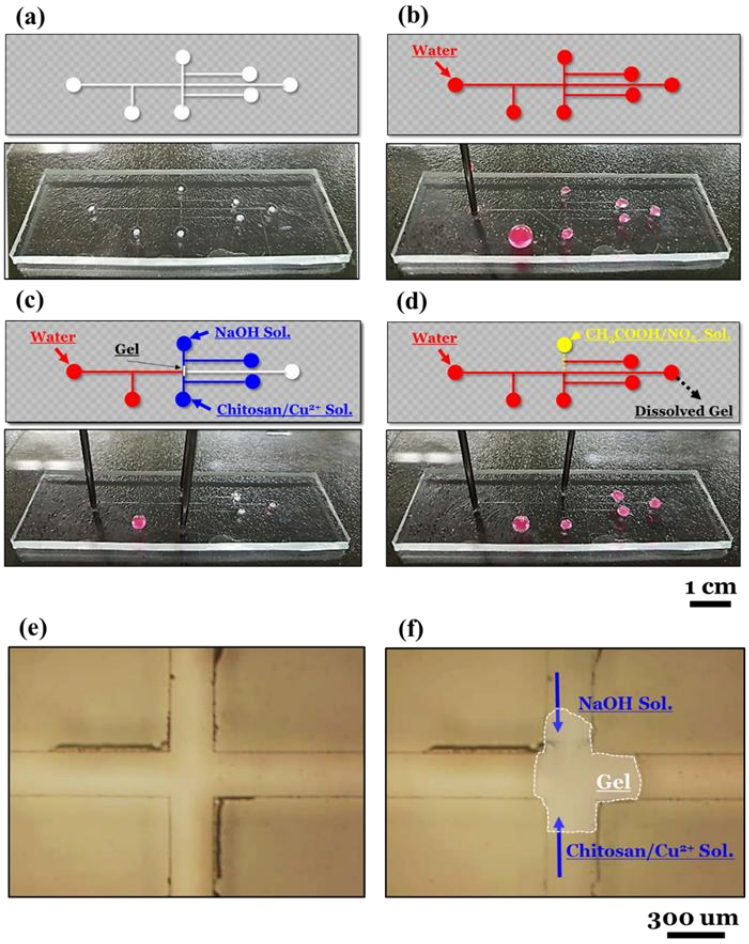

Figure 3.12. Microfluidic switch test: (a) Seven-hole microfluidic channel using patterned PDMS on glass. The channel dimensions were fixed as 300 um (width) and 50 um (depth). (b) Initial water flow check with a rate of 150 ul/min before the switch test. (c) The channel was closed by the gelation of chitosan/Cu^{2+} near the intersection. All of the water started to flow along the detour route in 5 sec. (d) The channel opened in 15 sec due to the dissolution of the chitosan/Cu^{2+} hydrogel using the CH_3COOH/NO_2^- aqueous solution. (e) Microscopic image of the intersection before the switch test. (f) Microscopic image of the intersection after closing. The hydrogel is indicated by the white box to describe it more clearly.

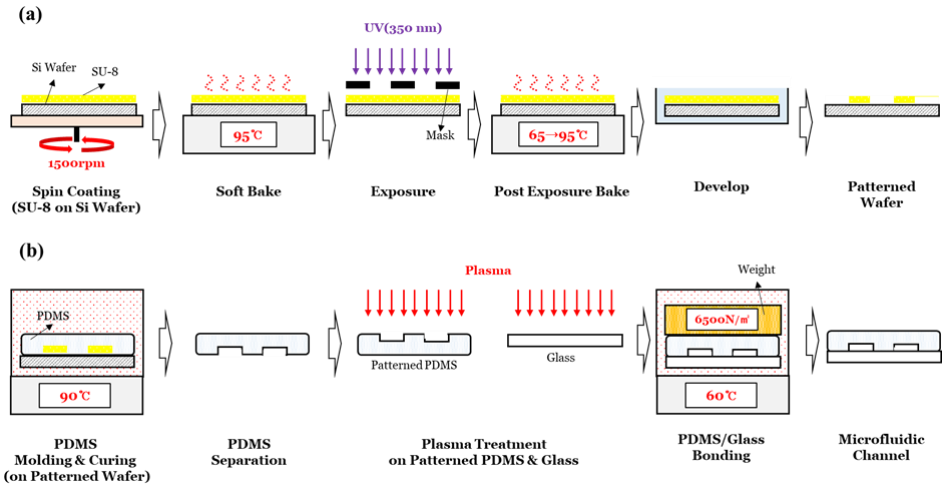

Figure 3.13. Schematic description of the fabrication of the microfluidic channel: (a) Patterned Si wafer (b) microfluidic channel.

3.4. Conclusion

In summary, dominant factors which influence the rates of the reversible crosslinking of chitosan/Cu^{2+} hydrogels were studied experimentally. Rapid gel formation could be achieved when the concentration of OH^- increased regardless of the concentration of Cu^{2+}, mainly due to the higher diffusion rate of OH^-, which deprotonated NH_3^+ to NH_2. Apart from the gelation rate, Cu^{2+} helped to realize gel characteristics quickly. Contrary to gelation, a decrease in the pH level was required to power the dissolution rate with the accelerated protonation of NH_2 to NH_3^+. Furthermore, NO_2^-, which has strong affinity to metal ions, helped to disintegrate the chitosan/Cu^{2+} hydrogel well. This enhanced the dissolution rate of the chitosan/Cu^{2+} hydrogel. Even though the affinity of NH_2 to metal ions (Mn^{2+}, Fe^{3+}, and Ca^{2+}) apparently affected the dissolution as well as the gelation, a phase transition of the chitosan/metal−ion hydrogel was similarly controlled by the factors such as NaOH, pH, and NO_2^-. Finally, a fluidic switch was operated via the reversible crosslinking of chitosan/Cu^{2+} hydrogels. The gel which formed at a high concentration of OH^- blocked the water flow perfectly. This gel could not be removed until an acidic aqueous solution was injected. Furthermore, NO_2^- dissolved in an acid aqueous solution shortened the operating time from closed to open. Moreover, a switch system could be successfully applied to a microfluidic channel as well. We expect that a controllable microfluidic device could be potentially applied to various fields such as hemostatic systems and trace metal analysis. Besides, this study provides a better understanding of the reversible crosslinking of the chitosan/metal−ion hydrogel and helps with the preparation of comprehensive strategies for the recycle process.

Reference

(1) Fu, J.; Yang, F.; Guo, Z. The chitosan hydrogels: From structure to function. New J. Chem. 2018, 42, 17162-17180.

(2) Gandini, A. Polymers from renewable resources: A challenge for the future of macromolecular materials. Macromolecules 2008, 41, 9491-9504.

(3) Nie, J.; Lu, W.; Ma, J.; Yang, L.; Wang, Z.; Qin, A.; Hu, Q. Orientation in multi-layer chitosan hydrogel: morphology, mechanism and design principle. Sci. Rep. 2015, 5, 7635.

(4) Berger, J.; Reist, M.; Mayer, J. M.; Felt, O.; Gurny, R. Structure and interactions in chitosan hydrogels formed by complexation or aggregation for biomedical applications. Eur. J. Pharm. Biopharm. 2004, 57, 35-52.

(5) Nisar, S.; Pandit, A. H.; Wang, L.-F.; Rattan, S. Strategy to design a smart photocleavable and pH sensitive chitosan based hydrogel through a novel crosslinker: A potential vehicle for controlled drug delivery. RSC Adv. 2020, 10, 14694.

(6) Hu, L.; Sun, Y.; Wu, Y. Advances in chitosan-based drug delivery vehicles. Nanoscale 2013, 5, 3103-3111.

(7) Sadat Ebrahimi, M. M.; Schönherr, H. Enzyme-sensing chitosan hydrogels. Langmuir 2014, 30, 7842-7850.

(8) Jang, J.; Kang, K.; Raeis-Hosseini, N.; Ismukhanova, A.; Jeong, H.; Jung, C.; Kim, B.; Lee, J. Y.; Park, I.; Rho, J. Self-Powered Humidity Sensor Using Chitosan-Based Plasmonic Metal-Hydrogel-Metal Filters. Adv. Opt. Mater. 2020, 8, 1901932.

(9) Kim, J.-N.; Lee, J.; Lee, H.; Oh, I.-K. Stretchable and self-healable catechol-chitosan-diatom hydrogel for triboelectric generator and self-powered tremor sensor targeting at Parkinson disease. Nano Energy 2021, 82, 105705.

(10) Lone, S.; Yoon, D. H.; Lee, H.; Cheong, I. W. Gelatin-chitosan hydrogel particles for efficient removal of Hg(ii) from wastewater. Environ. Sci.: Water Res. Technol. 2019, 5, 83-90.

(11) Upadhyay, U.; Sreedhar, I.; Singh, S. A.; Patel, C. M.; Anitha, K. L. Recent advances in heavy metal removal by chitosan based adsorbents. Carbohydr. Polym. 2021, 251, 117000.

(12) Xu, H.; Matysiak, S. Effect of pH on chitosan hydrogel polymer network structure. Chem. Commun. 2017, 53, 7373-7376.

(13) Liu, H.; Wang, C.; Zou, S.; Wei, Z.; Tong, Z. Simple, reversible emulsion system switched by pH on the basis of chitosan without any hydrophobic modification. Langmuir 2012, 28, 11017-11024.

(14) Wu, L.-Q.; Gadre, A. P.; Yi, H.; Kastantin, M. J.; Rubloff, G. W.; Bentley, W. E.; Payne, G. F.; Ghodssi, R. Voltage-dependent assembly of the polysaccharide chitosan onto an electrode surface. Langmuir 2002, 18, 8620-8625.

(15) Hu, P.; Raub, C. B.; Choy, J. S.; Luo, X. Modulating the properties of flow-assembled chitosan membranes in microfluidics with glutaraldehyde crosslinking. J. Mater. Chem. B 2020, 8, 2519-2529.

(16) Deng, Y.; Ren, J.; Chen, G.; Li, G.; Wu, X.; Wang, G.; Gu, G.; Li, J. Injectable in situ cross-linking chitosan-hyaluronic acid based hydrogels for abdominal tissue regeneration. Sci. Rep. 2017, 7, 2699.

(17) Luo, X.; Berlin, D. L.; Betz, J.; Payne, G. F.; Bentley, W. E.; Rubloff, G. W. In situ generation of pH gradients in microfluidic devices for biofabrication of freestanding, semi-permeable chitosan membranes. Lab Chip 2010, 10, 59-65.

(18) Choudhary, R. C.; Kumaraswamy, R. V.; Kumari, S.; Sharma, S. S.; Pal, A.; Raliya, R.; Biswas, P.; Saharan, V. Cu-chitosan nanoparticle boost defense responses and plant growth in Maize (Zea mays L.). Sci. Rep. 2017, 7, 9754.

(19) Nie, J.; Wang, Z.; Hu, Q. Chitosan hydrogel structure modulated by metal ions. Sci. Rep. 2016, 6, 36005.

(20) Rokugawa, I.; Tomita, N.; Dobashi, T.; Yamamoto, T. One-dimensional growth of hydrogel by a contact of chitosan solution with high-pH solution. Soft Mater. 2014, 12, 36-41.

(21) Dobashi, T.; Tomita, N.; Maki, Y.; Chang, C. P.; Yamamoto, T. An analysis of anisotropic gel forming process of chitosan. Carbohydr. Polym. 2011, 84, 709-712.

(22) Kim, K.; Ryu, J. H.; Lee, D. Y.; Lee, H. Bio-inspired catechol conjugation converts water-insoluble chitosan into a highly water-soluble, adhesive chitosan derivative for hydrogels and LbL assembly. Biomater. Sci. 2013, 1, 783-790.

(23) Kurita, K.; Yoshino, H.; Nishimura, S.-I.; Ishii, S. Preparation and biodegradability of chitin derivatives having mercapto groups. Carbohydr. Polym. 1993, 20, 239-245.

(24) Alves, N. M.; Mano, J. F. Chitosan derivatives obtained by chemical modifications for biomedical and environmental applications. Int. J. Biol. Macromol. 2008, 43, 401-414.

(25) Zeng, R.; Fu, H.; Zhao, Y. Synthesis of novel biomimetic zwitterionic phosphorylcholine-bound chitosan derivative. Macromol. Rapid Commun. 2006, 27, 548-552.

(26) Yan, K.; Xu, F.; Wang, C.; Li, Y.; Chen, Y.; Li, X.; Lu, Z.; Wang, D. A multifunctional metal-biopolymer coordinated double network hydrogel combined with multi-stimulus responsiveness, self-healing, shape memory and antibacterial properties. Biomater. Sci. 2020, 8, 3193-3201.

(27) Corsello, S.; Fulgenzi, A.; Vietti, D.; Ferrero, M. E. The usefulness of chelation therapy for the remission of symptoms caused by previous treatment with mercury-containing pharmaceuticals: a case report. Cases J. 2009, 2, 1626.

(28) Origin of color in complex ions, 2021. https://chem.libretexts.org/@go/page/3707.

(29) Spectrochemical series, 2021. https://chem.libretexts.org/@go/page/183320.

(30) Bégin, A.; Van Calsteren, M.-R. Antimicrobial films produced from chitosan. Int. J. Biol. Macromol. 1999, 26, 63-67.

(31) Richens, D. T. Ligand substitution reactions at inorganic centers. Chem. Rev. 2005, 105, 1961-2002.

(32) Timmons, A. J.; Symes, M. D. Converting between the oxides of nitrogen using metal-ligand coordination complexes. Chem. Soc. Rev. 2015, 44, 6708-6722.

(33) Kaim, W.; Das, A.; Fiedler, J.; Záliš, S.; Sarkar, B. NO and NO_2 as non-innocent ligands: A comparison. Coord. Chem.

Rev. 2020, 404, 213114.

(34) Baker, A. T. The Ligand Field Spectra of Copper(II) Complexes. J. Chem. Educ. 1998, 75, 98−99.

(35) Blake, A. J.; Hill, S. J.; Hubberstey, P. Unique cationic, neutral and anionic copper(II) nitrite species in a single compound. Chem. Commun. 1988, 15, 1587−1588.

(36) Chandra Maji, R.; Mishra, S.; Bhandari, A.; Singh, R.; Olmstead, M. M.; Patra, A. K. A Copper(II) Nitrite That Exhibits Change of Nitrite Binding Mode and Formation of Copper(II) Nitrosyl Prior to Nitric Oxide Evolution. Inorg. Chem. 2018, 57, 1550−1561.

(37) Roger, I.; Wilson, C.; Senn, H. M.; Sproules, S.; Symes, M. D. An investigation into the unusual linkage isomerization and nitrite reduction activity of a novel tris(2−pyridyl) copper complex. R. Soc. Open Sci. 2017, 4, 170593.

(38) Beebe, D. J.; Moore, J. S.; Yu, Q.; Liu, R. H.; Kraft, M. L.; Jo, B.−H.; Devadoss, C. Microfluidic tectonics: A comprehensive construction platform for microfluidic systems. Proc. Natl. Acad. Sci. U.S.A. 2000, 97, 13488−13493.

(39) Sugiura, Y.; Hirama, H.; Torii, T. Fabrication of microfluidic valves using a hydrogel molding method. Sci. Rep. 2015, 5, 13375.

(40) Satarkar, N. S.; Zhang, W.; Eitel, R. E.; Hilt, J. Z. Magnetic hydrogel nanocomposites as remote controlled microfluidic valves. Lab Chip 2009, 9, 1773−1779.

(41) Sershen, S. R.; Mensing, G. A.; Ng, M.; Halas, N. J.; Beebe, D. J.; West, J. L. Independent optical control of microfluidic valves formed from optomechanically responsive nanocomposite

hydrogels. Adv. Mater. 2005, 17, 1366-1368.

(42) Lin, S.; Wang, W.; Ju, X.-J.; Xie, R.; Chu, L.-Y. A simple strategy for in situ fabrication of a smart hydrogel microvalve within microchannels for thermostatic control. Lab Chip 2014, 14, 2626-2634.

(43) Wu, J.; Lin, Y.; Sun, J. Anisotropic volume change of poly(n-isopropylacrylamide)-based hydrogels with an aligned dual-network microstructure. J. Mater. Chem. 2012, 22, 17449-17451.

(44) Xia, Y.; Whitesides, G. M. Soft lithography. Angew. Chem., Int. Ed. 1998, 37, 550-575.

(45) Mata, A.; Fleischman, A. J.; Roy, S. Characterization of polydimethylsiloxane (PDMS) properties for biomedical micro/nanosystems. Biomed. Microdevices 2005, 7, 281-293.

(46) Wang, J.; Chen, W.; Sun, J.; Liu, C.; Yin, Q.; Zhang, L.; Xianyu, Y.; Shi, X.; Hu, G.; Jiang, X. A microfluidic tubing method and its application for controlled synthesis of polymeric nanoparticles. Lab Chip 2014, 14, 1673-1677.

(47) Ianovska, M. A.; Mulder, P. P. M. F. A.; Verpoorte, E. Development of small-volume, microfluidic chaotic mixers for future application in two-dimensional liquid chromatography. RSC Adv. 2017, 7, 9090-9099.

Chapter 4. Conclusion

In this dissertation, phase transitional gels were studied in order to demonstrate that hydrogels can be more practical and facilely-use. Especially, precisely controlled phases and their characterizations quantitatively supported the results. In relation to applications fields, adhesives and recyclable heavy metal removal system were developed.

First, PAA/BPEI complexes have been utilized as strong and facile adhesives based on precisely controlled phase and rheological analysis. Coacervate was suitable for a polyelectrolyte coating solution, and the gel layer could be easily loaded using a pH-induced phase transition. Then, it was found that a higher viscous phase led to more intensive adhesion strength of polyelectrolytes. In addition, thermal treatment helped to achieve a commercial level of adhesion strength, which was accomplished by conversion from carboxylic acid to amide. Even though a more in-depth study on the adhesion mechanism is required, we expect that the coacervate coating system could potentially be applicable to the polyelectrolyte deposition fields including adhesives, actuators, and barriers.

Second, reversible crosslinking of chitosan/Cu^{2+} complexes have been comprehensively studied. Especially, the dissolution process was mainly covered in order to realize recyclable materials. Contrary to gelation, a decrease in the pH level was required to power the dissolution rate with the accelerated protonation of NH_2 to NH_3^+. Furthermore, NO_2^-, which has strong affinity to metal ions, helped to disintegrate the chitosan/Cu^{2+} hydrogel well. This enhanced the dissolution rate of the chitosan/Cu^{2+} hydrogel. Lastly, a microfluidic switch was newly applied via the reversible crosslinking of chitosan/Cu^{2+} hydrogels. A controllable microfluidic device was expected to be potentially applied to various fields such as hemostatic systems.

Abstract in Korean

하이드로젤의 특별하고 유용한 특성을 활용하기 위해 많은 연구 결과들이 보고되고 있다. 예를 들어, 이중 가교 방식은 하이드로젤의 약하고 잘 부셔지는 단점을 개선하는데 중요한 역할을 하였고, 소수성 재료 코팅을 통해 수분을 잃는 문제도 극복되고 있다. 또한, 생체 적합성, 신축성, 그리고 외부 환경에 대한 반응성을 활용한 다양한 방면에서의 응용 연구도 흥미로운 부분이다. 하지만, 실험실을 벗어나 상업적으로 적용되고 유용하게 사용하기 위해서는 하이드로젤을 경쟁력 있고 대량으로 제조하는 방법에 대해서 적극적인 고민이 필요하다. 더 나아가, 친환경 재료로 부각되고 있는 하이드로젤의 장점중 하나인 재활용을 구현할 수 있는 공정 시스템을 설계하는 것도 앞으로 해야 할 과제이다.

이 논문에서는 하이드로젤의 상 전이 연구를 통해 이 재료를 보다 유용하게 사용할 수 있는 방안을 제시하고자 한다. 정밀한 상 제어 통한 평가 결과 하이드로젤은 더 쉽고 간편하게 활용될 가능성을 갖고 있으며, 재활용 시스템을 설계하는데 재료 측면에서 고민할 수 있는 점이 있다고 판단된다. 이들을 접착제와 중금속 제거 시스템을 통해 집중적으로 논의할 것이다. 추가로, 상 전이가 가능한 하이드로젤을 통해 유체 흐름을 제어하는 응용 분야를 새롭게 제시할 것이다.

첫 번째 장에서는 강하고 사용하기 편리한 접착제를 구현해 보고자 했으며, 폴리아크릴릭엑시드와 브랜치드 폴리에틸렌이민으로 구성된 폴리일렉트로라이트의 상 제어를 활용하였다. 반대 전하를 갖는 고분자 콜로이드가 모여 만들어진 코아서베이트는 폴리일렉트로라이트를 기판에 도포하는데 유용했으며, pH 제어를 통해 젤로 전환할 수도 있었다. 결과적으로 균일한 접착제 도포 및 상 제어를 통해 접착력을 정량적으로 분석하였고, 코아서베이트 보다 젤에서 강한 접착 특성을 확인했다. 또한, 열처리 통한 아마이드 결합 형성을 통해 젤의 접착력을 대폭 개선할 수 있었으며 (2.4 MPa), 상용 제품 수준을 구현하였다. 본 연구를 통해 폴리일렉트로라이트의 응용 범위와 방식이 넓어질 수 있다는 기대감과 함께, 이 재료의 부족한 점을 극복하는 노력이 더 필요하다는 것도 다시 한 번 확인하였다.

두 번째 장에서는 키토산/구리 사이의 가역적인 가교 방식을 통해 재활용할 수 있는 중금속 제거 시스템에 대해 연구했다. 기존의 연구 결과와 달리 배위 결합으로 구성된 키토산/구리 하이드로젤을 빠르게 녹이는데 관심을 가졌다. 이는 하이드로젤을 재활용하기 위한 필수적인 공정 단계로 중요하다고 생각한다. 유기 분자의 금속 이온 친화도를 활용했으며, 나이트라이트를 통해 키토산/구리 하이드로젤의 녹는 속도가 대폭 개선되었다. 마지막으로 고분자/금속 사이의 가역적인 가교 방식을 통해 미세 유체 제어 시스템에도 처음으로 적용하고 검증하였다. 본 연구는 기존의 관심과 달리 하이드로젤을 어떻게 하면 빠르고 잘 녹여낼 수 있을지에 대해 심도 있게 고민했다. 재활용 측면에도 장점이 있는 하이드로젤의 발전을 위해 젤 기반의 제품 사이클을 다시 한 번 설계하고, 종합적인 연구가 필요하다고 생각한다. 마지막으로, 가역적인 상 전이를 활용하여 유체 흐름을 제어할 수 있음을 검증했으며, 하이드로젤의 새로운 응용 분야로 제시하였다.

Keyword: 하이드로젤, 상 전이, 폴리일렉트로라이트, 배위 결합 화합물, 접착제, 미세 유체 제어

Student Number: 2019-33177